The hypertidal Santa Cruz – Chico River Estuary (South Patagonia, Argentina): A hybrid ria-type system under extreme tides, arid climate and active uplift

Bernadette Tessier, Jean-Yves Reynaud, Jose Cuitiño, Roberto Scasso, Léo Pancrazzi, Maria Duperron, Pierre Weill, Viviane Bout-roumazeilles, Eric Armynot Du Châtelet, Anjana Kuinkel, et al.

The hypertidal Santa Cruz – Chico River Estuary (South Patagonia, Argentina): A hybrid ria-type system under extreme tides, arid climate and active uplift

Bernadette Tessier, Jean-Yves Reynaud, Jose Cuitiño, Roberto Scasso, Léo Pancrazzi, Maria Duperron, Pierre Weill, Viviane Vbr Bout-Roumazeilles, Eric Armynot Du Châtelet, Anjana Kuinkel, et al.

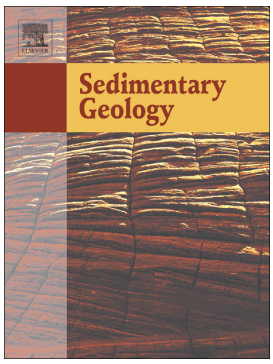

The hypertidal Santa Cruz – Chico River Estuary (South Patagonia, Argentina): A hybrid ria-type system under extreme tides, arid climate and active uplift

Bernadette Tessier, Jean-Yves Reynaud, Jose I. Cuitiño, Roberto A. Scasso, Léo Pancrazzi, Maria Duperron, Pierre Weill, Viviane Bout-Roumazeilles, Eric Armynot du Châtelet, Anjana Kuinkel, Thibaud Lortie, Laurent Dezileau

PII: S0037-0738(24)00151-9

DOI: https://doi.org/10.1016/j.sedgeo.2024.106728

Reference: SEDGEO 106728

To appear in: *Sedimentary Geology*

Received date: 16 April 2024

Revised date: 29 July 2024

Accepted date: 1 August 2024

Please cite this article as: B. Tessier, J.-Y. Reynaud, J.I. Cuitiño, et al., The hypertidal Santa Cruz – Chico River Estuary (South Patagonia, Argentina): A hybrid ria-type system under extreme tides, arid climate and active uplift, *Sedimentary Geology* (2024), https://doi.org/10.1016/j.sedgeo.2024.106728

The hypertidal Santa Cruz – Chico River Estuary (South Patagonia, Argentina): a hybrid ria-type system under extreme tides, arid climate and active uplift

Bernadette Tessier[1*], Jean-Yves Reynaud[2], Jose I. Cuitiño[3], Roberto A. Scasso[4], Léo Pancrazzi[1], Maria Duperron[4], Pierre Weill[1], Viviane Bout-Roumazeilles[2], Eric Armynot du Châtelet[2], Anjana Kuinkel[2], Thibaud Lortie[1], Laurent Dezileau[1]

1 Université de Caen Normandie, CNRS, Univ Rouen Normandie, Normandie Univ, UMR 6143 M2C, 14000 Caen, France

2 Univ. Lille, CNRS, Univ. Littoral Côte d'Opale, UMR 8187 LOG, F 59000 Lille, France

3 IPGP-CENPAT-CONICET - Puerto Madryn, Chubut, Argentina

4 IGeBA, Dpto. de Cs. Geológicas, Universidad de Buenos Aires - CONICET, Argentina

* corresponding author: bernadette.tessier@unicaen.fr

Abstract

The present study focuses on the morphosedimentary organization and sediment infilling stratigraphy of one of the largest estuaries of southern Patagonia in Argentina. With a tidal range up to 12 m, the area is subject to extreme tidal conditions, combined with moderate offshore wave climate, strong and constant westerly winds, and contrasted water and sediment discharges from the two tributaries of the estuary, the Santa Cruz and Chico Rivers. The estuarine valley is entrenched in the Patagonian coastal plateau due to significant uplift. On the basis of sediment facies (sedimentary structures, grain size, geochemistry, mineralogy), meiofauna (foraminifera and testate amoebae), morphological changes and shallow geophysics (high-resolution seismic reflection, ground-penetrating radar) data, the Santa Cruz-Chico River system is defined as a hybrid system comprising a tide-influenced fluvial mouth (the Santa Cruz River) and a tide-dominated estuary (the Chico River estuary), both converging towards an elongated subtidal ria-type estuarine basin. River-supplied sands and muds by-pass the estuarine basin and are exported offshore where they settle and form an ebb-tidal delta. Sediments in the Santa Cruz-Chico River valley mainly consists of Pleistocene lowstand fluvial gravels resting on the regional

Miocene substrate, and thin early Holocene transgressive deposits, deeply incised by a tidal ravinement surface that developed during the highest Holocene sea-level at ca 7500 yr. BP. After the maximum stillstand, relative sea level fell and a competition occurred between erosion, promoted by water depth decrease, and deposition, favoured by tidal prism reduction. At present, sediment by-passing and offshore sediment export are the dominant processes. The very large size of the ebb-tidal delta, which expands on the continental shelf, suggests that this situation has prevailed for a very long time.

Key-words: South America, incised-valley, tides, sediment by-pass, geophysics, Holocene stratigraphy

1. Introduction

Estuarine systems are major sedimentary components at the land-to-sea transition, sensitive to changes occurring both in the catchments and at the coast and marine approaches. These changes, either of natural and anthropogenic origins, induce fluctuations in fluvial, wave and tide hydrodynamics, and concomitantly in sediment transport and supply. In order to better understand estuary morphodynamic behaviour, as well as to guide predictive reconstruction of sedimentary infill of incised valleys, generally associated with estuarine systems, conceptual models of estuarine morphosedimentary organization have been proposed, distinguishing two types of estuaries according to the hydrodynamics prevailing at the estuary mouth: tide-dominated estuaries -TDE- and wave-dominated estuaries -WDE (Dalrymple et al., 1992). TDE and WDE are end-members bounding a range of intermediate estuarine morphologies depending on the degree of mixing of the different hydrodynamics. Since the classification of Dalrymple et al. (1992) depends on the dominant agent, wave or tide, at the mouth, estuaries located in macro- to even hypertidal coastal regions are not necessarily tide-dominated. In areas where large amounts of nearshore coarse-grained sediment (sands to pebbles) are available and where wave regime is powerful enough to control their cross-shore and longshore transport, sandspits can construct at estuarine mouths, leading to the development of a WDE. Rock-bound estuaries as defined by Fitzgerald et al. (2000) may show common characteristics with WDE when their mouth is barred due to bedrock morphology, acting similarly to a coastal barrier. As a result of combined hydrodynamics, topography and sediment supply, a larger variety of incised valley-fill models thus arises (Chaumillon et al., 2010).

Archer (2013) examined the morphosedimentary characteristics of coastal sites that have the largest tidal ranges in the world, i.e., which usually exceed 8 to 10 m. These sites include seaways, embayments and estuaries. Most of them are located along passive margins, in the Northern Hemisphere (Archer and Hubbard, 2003). Only two coastal sites are located in the Southern Hemisphere: The Kimberley coast of NW Australia; the Southern Patagonian coast owing to the very large width (about 800 km until the 200 m isobath) of the shelf in this southernmost portion of the South America Atlantic margin (Fig. 1A). In the estuaries and embayments located along this coast, tidal ranges reach up to 11 m (Hypertidal C according to Archer, 2013) bringing projects to evaluate the potential of tidal power harnessing at the estuary mouths (Bindelli et al., 2023). One of these estuaries is the Santa Cruz - Chico River (SC-CR) estuary.

In the framework of a Franco-Argentinian collaborative project initially aimed at studying the infilling stratigraphy of hypertidal estuaries, we performed field surveys in the largely unexplored SC-CR estuary including morphology, sedimentology, and geophysics (seismic reflexion, Ground Penetrating Radar) investigation. In light of the data collected, we discuss in the present paper how this hypertidal estuary is organized in terms of sedimentary facies and environments as well as of sediment transport and infilling, and how it can be categorized as a hybrid system combining characteristics of rock-bound estuaries, resembling in shape to wave-dominated estuaries, and of tide-dominated (to wave-influenced) estuaries. A prime interest of the hypertidal SC-CR estuary owes to the fact that it lies in an arid region, influenced by contrasted seasonal changes in water runoff and sediment supply, and subject to tectonic uplift. Our goal is to highlight how these tidal, climatic and tectonic characteristics did influence its Holocene evolution, in order to allow comparison with other hypertidal systems already documented, mostly located in the Northern Hemisphere and for which the influence of fluvial regime is generally poorly considered (Dalrymple and Zaitlin, 1994; Chaumillon et al., 2010; Tessier, 2012; Tessier et al., 2012). Moreover, almost all case studies belong to transgressive contexts, few examples only describing estuaries subject to uplift and relative sea-level fall. Studies generally concern small estuaries, not necessarily tide-dominated (e.g., Sakai et al., 2006), and focus on the record of earthquake-induced subsidence or co-seismic uplift events into the sediment infill (e.g., Barryman et al., 1991; Nelson et al., 2009).

2. The Santa Cruz - Chico River estuary

2.1. Geological context

The SC-CR estuary is one of the five estuaries located along the Patagonian coast of Argentina, between the Chubut estuary to the north and the Gallegos estuary some 1000 km to the south (Fig. 1A). All but the Chubut are classified as rias by Castaing and Guilcher (1995) and Goudie (2018), incised into Miocene or Jurassic substrate. The SC-CR, Coyle (or Coig) and Gallegos estuaries are located at the mouth of steppe rivers in southeast Santa Cruz province (Piccolo and Perillo, 1999).

The SC-CR estuary lies at the confluence of two drainage basins: the Santa Cruz River basin and the Chico River basin. Both drainage basins have their headwaters in a high relief zone at the Southern Patagonian Andes, although the Chico River headwaters are relatively shifted eastward in relation to the Santa Cruz basin (Fig. 1B). The Santa Cruz headwaters drain on structurally uplifted terrains formed by late Palaeozoic metasedimentary basement and Jurassic acidic volcanic rocks, and is directly connected to the Southern Patagonian Ice Field (Fig. 1B). Cretaceous black shales and siliciclastic sandstones of the rift to foreland Austral-Magallanes Basin are an important surface component for this area (Fig.1B; Ghiglione et al., 2016; Cuitiño et al., 2019). In contrast, the headwaters of the Chico River basin show little proportion of basement rocks, and a higher proportion of younger siliciclastic sedimentary rocks. Glaciogenic deposits are also a common geological unit in both headwaters, especially in the Santa Cruz River basin. Eastward, in the middle to lower reaches of their drainage basins, the Santa Cruz and Chico rivers are incised into a relatively flat, undeformed terrain composed of fine-grained foreland Cenozoic siliciclastic to volcaniclastic rocks as well as late Cenozoic backarc basaltic lava beds that cover large parts of the high plateaus (Fig. 1B). In this intermediate zone, extensive fluvial terraces mantled by gravel deposits formed during the late Neogene to Quaternary fluvial incision. Near their joint mouth, both valleys are incised into the early Miocene marine Monte León and terrestrial Santa Cruz Formations (Fig. 1B) (Sacomani et al., 2012). These two formations constitute part of the sedimentary infill of the Austral Basin that was formed on the foreland side of the Southern Patagonian Andes (Cuitiño et al., 2016; Parras and Cuitiño, 2018). Most of these Miocene formations are made mostly of poorly cemented fine-grained silty to sandy successions, the sediment of which originated for a significant proportion from the fall and reworking of Andean volcanic ashes.

This Miocene substrate, that gently dips to the southeast (less than 5º, Cuitiño et al., 2016; Parras and Cuitiño, 2018), is widely covered by the glacio-fluvial Plio-Pleistocene fluvial terrace gravels assigned to the Patagonian Shingle Formation, informally known as the "Rodados Patagónicos" (Martinez and Kutschker, 2011) which are incised as well by the Santa Cruz and Chico Rivers.

Due to subcrustal processes such as lithospheric thinning and dynamic topography tectonic, probably secondarily to glacio-isostatic adjustment, the study area is subject since the late Miocene to a significant uplift (Ávila et al., 2023), featured along the Atlantic coastal zone by raised marine terraces (Pedoja et al., 2011). Pleistocene uplift rate at the study site is estimated around 0.11-0.12 mm/yr (Pedoja et al., 2011). As a consequence, during the last post-glacial transgression, Holocene sea level reached a maximum altitude of about 8-9 m above present-day mean sea level at around 7500-7000 y. BP (Pedoja et al., 2011; Zanchetta et al., 2014). According to several studies along Patagonian coasts on marine terraces and beach ridges, the subsequent relative sea level fall is found to be stepped, with periods of more rapid falls and periods of stillstands (Rostami et al., 2000; Sheldman and Radtke, 2010; Zanchetta et al., 2014).

2.2. General morphology of the SC-CR estuary

The SC-CR estuary is a complex system made of the lower reaches of the Santa Cruz River and the Chico River merging into an intermediate basin, 25 km long down to the outlet to the Atlantic Ocean (Figs. 1C, 2). Tidal and salinity variations are recorded up to 10-15 km upstream the confluence. In the next sections, reference to the Chico and Santa Cruz Rivers only concerns those estuarine segments of these rivers (Figs. 1C, 2). The Chico River has a well-defined elongated funnel shape over a distance of 20 km from the confluence to the National Road 3 bridge, with a width ranging from almost 3 km at the confluence to 100 m at the bridge. From the bridge to the confluence, the system evolves rapidly from a meandering single channel to a sinuous to braided channel network. All along the Chico River, the main channel shows at low tide a quite constant width of 100-200 m. Meander wave length is *ca.* 1 km. The width of the Santa Cruz River at the confluence is comparable to the Chico River width, *i.e.*, 3–3.5 km, decreasing upstream over a distance of 18 km until a width of 1–1.5 km. The funnel-shaped estuary shows a large-scale sinuosity of *ca.* 10 km wavelength. The Santa Cruz River channel, like the

one of the Chico River, has a more or less constant width, ranging from 0.5 to 1 km. The system evolves from a single river channel floored by braided to anastomosed bars in the upper portion, to a single channel flanked by large tidal flats in the lowermost reach.

The intermediate basin between the confluence and the outlet has an almost constant width of 5.5-6 km over its 25 km of length. In the middle of the basin emerges the 4 km long, shore-parallel, Leones Island, probably developed on a bedrock shoal. The intermediate basin narrows significantly close to the mouth where the outlet is only 2 km wide, and less than 2 km long, widening suddenly to the open sea. The Chico River and the intermediate basin have the same NW-SE orientation, whereas the Santa Cruz River is almost W-E oriented (Fig. 1C).

A general geomorphological characteristic of the SC-CR estuary is the asymmetry of altitude along both sides (Fig. 2). The NE side of the intermediate basin and Chico River, cut into the lowest fluvial terrace ("Rodados Patagónicos"), has a much lower elevation, of about 15 m, than the SW side of the intermediate and southern side of Santa Cruz River, characterized by high cliffs incised into the Miocene substrate, about 50 m high along the Santa Cruz River, rising until 110 -115 m toward the confluence and along the intermediate basin (Fig. 2). The northern side of the Santa Cruz River cuts the fluvial gravel terraces at an altitude of about 20 to 30 m, although lying very close, locally less than 1 km, to the 120 m high Miocene cliffs. The altitude of the SW side of the Chico River ranges from 40 to 110 m, cut into the Miocene and fluvial terraces.

Active tidal flats along the estuary, including the gravel beaches on the northern side of the inlet, are locally fringed by low terraces incised by multiple channels forming a dendritic tidal channel network. Their altitude is around 8-10 m or less (Fig. 2). Some of these terraces, like the main one developed on the northern side of the Santa Cruz River (Fig. 1C), are covered by aeolian silts and dusts, forming locally nebkhas, and fringed in some places by gravel ridges. According to their altitude, these tidal flats could be related to the Holocene maximum sea level, at around 7500 y. BP., maybe at 3500 y. BP (Rutter et al., 1989; Rostami et al., 2000; Schellmann and Radtke, 2010; Zanchetta et al., 2014), and are probably inactive nowadays. However, the main terrace along the Santa Cruz River is possibly flooded occasionally during the highest fluvial levels combined with high spring tides.

2.3. Main hydrographic characteristics

The Santa Cruz River is the main river of Patagonia, delivering 39% of the total mean annual Patagonian discharge (Depetris et al., 2005). It was explored by Charles Darwin in April 1834 during the second campaign of the *HMS Beagle* in Patagonia. It has a length of 380 km and a catchment basin of 24,000 km^2. It is directly connected upstream to Lake Argentino (Fig. 1B). The seasonal fluctuations of the lake water level control the river discharges (Pasquini and Depretis, 2011). The mean annual water discharge is about 750 $m^3\ s^{-1}$, with an average maximum and minimum of 1280 and 280 $m^3\ s^{-1}$. Seasonal variability is relatively low, mostly controlled by snow and ice melt in the headwaters. However, due to the collapse of ice dams in upstream branches of the lake, water outbursts regularly occur (every 2-4 years), generally in March, resulting in higher discharge peaks (2500 $m^3\ s^{-1}$) (Pasquini and Depetris, 2011).

On the other side, the Chico River, with a length of about 550 km but a drainage basin of 16,800 km^2 is a smaller river, with a mean annual water discharge of 30 $m^3\ s^{-1}$ (Gaiero et al., 2003).

With respect to sediment supply, concentration of suspended material is higher in the Chico River, with values of a few 100 mg l^{-1}, whereas in the Santa Cruz concentrations reach only a few 10 mg l^{-1} (Depetris et al., 2005).

2.4. Wave, wind and tidal dynamics

The climate in the study area is temperate cold with an average annual temperature of 8 °C, and arid to semi-arid with an average annual rainfall of less than 200 mm. The main characteristics of the Patagonian climate are the intense winds that blow almost permanently from the west. Because moisture is trapped on the Pacific side of the Andes, they are dry winds transporting significant dust amounts. For this reason, Patagonia is the first dust supplier of South America (Prospero et al., 2002; Gaiero et al., 2007). These westerly winds induce active erosion of the poorly cemented Miocene substrate, including of the cliffs along the estuary, as well as numerous, more or less circular, depressions on top of the Miocene plateau. They also provoke substantial sand transport on the tidal flats at low tide.

In addition, due to the quasi-permanent windy climate, agitation on the estuary water surface can be important, especially during tidal flood stages, when the westward average direction of flood currents is contrary to the dominant westerly winds. Moreover, the strongest westerlies probably retard flood tidal current and enhance ebb one, although no measurements and modelling are available to confirm it (Piccolo and Perillo, 1999). Offshore, significant wave height rarely exceeds 3 m. Mean significant wave height in front of the inlet, based on a global ocean physics reanalysis between 2010 and 2020 (data source: Copernicus Marine Data Store, 0.2° horizontal resolution), ranges from 0.5 to 1 m without major differences between seasons. The wave directions are evenly distributed from the north-east to the south-west with a small dissymmetry to the south-west. The short-period swells (less than 9 s) from south-west to south directions represent 22% of the sea state and mainly occur during the summer. The highest waves are generated during this summer period, where 3% of the wave heights ranges between 2 and 3 m, reaching occasionally maximum heights of 4.5 m. The longest swells have periods ranging from 10 to 17 s with directions from north-east to south-east, representing 13% of the sea state. The wave height of these long swells usually remains below 1 m.

Tidal dynamics in the SC-CR estuary is governed by the regional hypertidal range, reaching up to 12 m at Punta Quilla, located 4.5 km upstream of the mouth (Servicio de Hidrografía Naval: http://www.hidro.gov.ar). The hypertidal range of Southern Patagonia is related to the very large extension of the Patagonian shelf, and to the large concave morphology of the coastal region (Archer, 2013), named Bahia Grande. The tidal regime is semi-diurnal with very low diurnal inequality, characteristic of the tidal wave of the Atlantic Ocean domain. Tidal currents are commonly faster than 1.5 m/s, reaching up to 4 m/s into the 2 km wide narrow inlet. The flood is generally the dominant current, but the ebb is dominant in the downstream half of the intermediate basin according to current velocity indications mentioned on the 1945 nautical map (Fig. 4B). According to measurements and numerical modelling, both performed in the framework of environmental studies related to two hydroelectric dam constructions upstream on the river, 185 km and 250 km of the SC-CR estuary outlet (Ezcurra and Schmidt, 2018; Schmidt et al., 2018), fluvial discharge has little influence on the intermediate basin water levels which are instead controlled by tidal fluctuations. The same occurs with bottom velocities, which are influenced by water discharge for less than 15 km downstream of Comandante Luis Piedrabuena city (Fig. 1C). These downstream limits of water discharge influences

on water levels and bottom velocities probably shift significantly downstream during water outbursts of the Santa Cruz. With respect to salinity, the influence of freshwater discharge extends until the outlet at low tide.

3. Materials and Methods

To accomplish our objectives, four field surveys for sedimentological, seismic and GPR investigation have been performed.

3.1. Sedimentological observations and sediment analyses

In addition to observations made at different sites to characterize sediment facies and depositional environments around the estuary, 18 superficial sediment samples were collected from intertidal areas of the inlet to the upstream reaches (Table 1, cf. figures in the result section for sample location) for grain-size, mineralogical, and geochemical analyses. Meiofauna content of 22 sediment samples (foraminifera and testate amoebae) was also examined (Table S1).

Grain-size analysis – Laser grain-size analyses were carried out for each sample using a Beckman-Coulter LS13320 (M2C Laboratory, France). Prior to analysis, in order to prevent flocculation, samples were suspended in deionized water and exposed to ultra-sound during the measurement for 90 s. Each sample was measured twice to ensure accurate and consistent results.

Sediment mineralogy – For bulk sediment analyses, the samples were first transformed into very fine powder using an agate microgrinder and then compacted as to form a solid pellet to be analyzed by XRD-scanning. The clay-size fraction (<2µm) was isolated by differential settling according to Stoke's law. X-ray diagrams were obtained using a Bruker D4 Endeavor (standard 30 kV and 30 mA) coupled to a Lynxeye fast detector. Clay sample was run three times between (1) air dried sample, (2) glycolated sample (saturation in ethylene glycol for 12 hours), and (3) heated sample (490°C for two hours). The proportion of each clay mineral (smectite, chlorite, illite and kaolinite) is determined using the main X-ray diffraction peaks (layer + interlayer) on X-ray spectra according to their crystallographic properties

(Brindley and Brown, 1980; Beny et al., 2020). All measurements and semi-quantitative estimations were processed using Highscore+ software (bulk samples) and MacDiff software (clay samples, Petschick et al., 1996). The index of Esquevin (Esquevin, 1969) corresponds to the ratio between the 5Å and the 10Å peak intensities (illite 5Å/10Å). The illite crystallinity corresponds to the peak width at mid-height.

Sediment geochemistry - Geochemical analysis was carried out using a hand-held Niton XL3t spectrometer (pXRF; Geoscience Montpellier Laboratory, France). Each measurement was taken for 150 s with the soil mode, which is the most suitable mode for unconsolidated sediments. Before measurements were taken, all samples were dried and grinded to < 63 µm using a mechanical agate mortar, and then prepared in classic XRF sample cups covered with a thin ultralene film. Elements above the limit of detection are Cl, K, Ca, Ti, Cr, Mn, Fe, Co, Zn, As, Rb, Sr, Zr, Ba, Pb.

Meiofauna content **–** The study of meiofauna aimed in completing the characteristics of depositional environments with a biological indication of marine or freshwater influences. Meiofauna analyses focused on two unicellular eukaryotes groups, foraminifera and testate amoebae. Twenty-two samples were selected due to their silty to medium sand grain size (preferential requirement of these protist occurrence). Samples were sieved through 315 and 50µm mesh. The intermediate fraction was then concentrated on trichloroethene in order to remove most of detrital denser grains. Foraminifera and testate amoebae were then all counted within the residue. Foraminifera species were identified at species level and named checked according to World Register of Marine Species (WORMS) (Hayward et al. 2020). Testate amoebae were identified according to Ogden and Hedley (1980).

3.2. Very-High Resolution Seismic reflection and Ground-Penetrating Radar investigations

Geophysical investigations (Fig. 3) were performed in order to get information on the long-term evolution of the estuary. A very high-resolution seismic survey using a boomer source (®IKB Seistec, M2C Lab.) was performed on board of the Surveillance and Rescue ship of the Argentine Navy Prefecture based in Puerto Santa Cruz. We collected a few kilometres of seismic lines into the intermediate basin (Fig. 3A). The Seismic Unix software was used for data processing, including pass band and swell filters. The first objective of the ground penetrating radar (GPR) survey was to study in detail the architecture

of various types of gravel spits and beach ridge barriers that form the estuary mouth system, and to draw conclusion on its late quaternary paleogeographic evolution (Pancrazzi, 2022; Pancrazzi et al., accepted**)**. For the present study, the purpose is to show more general architectural features in relation to the development of the beach ridges on both sides of the inlet. A GPR SIR-3000 system with a 400 MHz shielded antenna (M2C Lab), and GPR SIR-4000 system with a 350 MHz HS digital antenna (LOG Lab) were used to explore the gravel barrier system (Fig. 3B). The GRPPy software (Plattner, 2020) was used to process the GPR data. Altimetric corrections were possible thanks to DTMs available in the study area (source: IGN 2015 photogrammetry survey).

3.3. Morpho-bathymetric data

In order to evaluate the recent evolution of the estuary, morpho-bathymetric changes have been examined by comparing different documents. Sediment and bathymetric maps of the SC-CR estuary are very scarce. The oldest nautical map of the region we could find so far is from 1866, with inserts focussing on some of the main estuaries, including the SC-CR estuary (Fig. 4A). A 1:50000 scale nautical chart of 1945 is available for the whole intermediate basin, from the confluence to the shallow offshore (Fig. 4B). Recently, bathymetric data were collected by Ezcurra and Schmidt (2018) and Schmidt et al. (2018), allowing to reconstruct a Digital Elevation Model (Fig. 4C). Present-day morphological characteristics and sedimentary body planforms can be checked on satellite data, and more especially on images from the optical sensor of the Sentinel generation 2 satellites. The 2022, May 21 image has been taken during very low tide conditions and can be compared with the DTM (Fig. S1). Since old bathymetric maps only concern the intermediate basin, in order to depict changes along the Chico and Santa Cruz rivers, the oldest satellite image available on Google Earth, dated from 1970, has been used to be compared with the present-day situation (Fig. 4D, E).

4. Results

4.1. Recent morpho-bathymetric evolution of the estuary

The comparison between the oldest reliable map, i.e., the 1945 map (Fig. 4B) with the most recent data (Fig. 4C) clearly demonstrates that no significant changes in water depth occurred during the last nearly 80 yearsI. In terms of morphology, banks and channels remain of similar size and shape, and at the same location within the intermediate basin and at the confluence (Fig. 4B, C, Fig. S1). Although the 1866 map (Fig. 4A) is not very accurate, it shows a very similar morphology compared to the most recent ones, demonstrating the high stability of the estuary since at least 150 years.

The evolution into the Santa Cruz River and Chico River cannot be examined at this centennial time scale because the 1866 and 1945 nautical charts do not cover these areas. However, little differences are evidenced when the oldest satellite image from 1970 is compared with the most recent data (Fig. 4D, E). The Santa Cruz River looks very similar, with the same position and planform for the main channel and fluvial bars, and more or less the same extension of the tidal flats. In the Chico River the main channel has slightly evolved from a more braided planform to a more linear one, suggesting a less dynamic system.

The 2022 Sentinel image (Fig. S1) shows a well-developed suspended sediment plume that gets out from the inlet. The plume shape is consistent with the morphology decipherable on the nautical chart of 1945 (Fig.4B), shifted towards the south and with an elongated bank on its external side. This morphology, which is not visible on the DTM produced in 2016 (Fig. 4C, Fig. S1 for a direct comparison), probably due to the relatively too low density of bathymetric data used to reconstruct the model, indicates the presence of a sedimentary body settled down off the inlet and resembles an ebb-tidal delta.

4.2. Sedimentary environments and facies distribution

Depositional environments and sediment facies of supra- to intertidal (backshore/foreshore) domains display a large diversity all around the estuary. Into the intermediate basin and along the southern side of the Santa Cruz, most estuarine coastlines are characterized by gravel beaches and spits that generally occupy the upper intertidal domain (Fig. 5B, C, F, H), or only the uppermost beachfaces and terraces. In the intertidal prolongation, mud flats are well-developed, especially along the SW side of the intermediate basin. When gravel beaches are reduced to uppermost beach terraces, a complete

sequence from salt marshes to intertidal mixed to mud flats can develop. This is the case for example along the shore between Puerto Santa Cruz and Punta Quilla (Fig. 5E). Mixed and mudflats are made of thinly laminated and sometimes bioturbated facies (Fig. 6G, H). Approaching the inlet, close to Punta Quilla, shore-normal, erosional furrows, probably due to wave action, dissect the mudflats (Fig. 5F). The shore along the NE side of the intermediate basin is essentially gravelly, with very few places showing salt marshes and mud flats.

At the outlet of the Chico River, salt marshes and mud flats are particularly well developed on the NE side. On the opposite side, due to a small gravel spit anchored to the Miocene bedrock cape delineating the confluence, a salt marsh and mud flat succession is sheltered and well preserved (Fig. 5K). Along the Chico River, mud to sand flats (Fig. 5J) develop with respect to their distance with tidal channels, the planform of which is mainly meandering, slightly more anastomosed in the central area. Sand flats with ebb-oriented subaqueous subaqueous small to medium dunes, a few ten centimetres high, are more extended at the outer section (Fig. 5L). Sediment successions consist of heterolithic facies made of sand-mud couplets, centimetric in thickness. Some of the successions show clear cyclic patterns (Fig. 6B, C, E) suggesting tidal rhythmites (Tessier, 2023; Cuitiño et al., 2023; Lortie et al., 2024). Salt marsh successions display very regular beddings very likely corresponding to annual rhythmites (Fig. 6F).

Along the Santa Cruz River, sand- to mud flats are extensively developed along the northern side (Fig. 5M, N). Sand flats occupy most of the major “valley”, and are shaped by numerous bedforms such as subaqueous small to medium dunes close to the main tidal channel along the southern side. Dunes appear to be ebb-oriented. However, they are observed only at low tide, thus after ebb tidal current action. Mud flats occupy the uppermost part and are incised by tidal creeks originated at the salt marshes. Heterolithic tidal facies, locally well-defined tidal rhythmites, are the main component of the mud flat deposits (Fig. 6D). Bedding into the salt marsh successions suggests as well tidal facies, probably of annual origin, similarly to those located at the outlet of the Chico River. A few kilometres upstream, sand to mud flat environments progressively disappear, being replaced by gravel bars in the channel and gravel attached-banks (Fig. 5I). Tidal influences are marked by horse-shoe morphologies featuring flood barbs. Moreover, the Miocene bedrock locally crops out along the northern side of the river downstream of Comandante Luis Piedrabuena city (Fig. 5G).

Sand flats developing at the Rio Chico and Santa Cruz outlets join together at the confluence, forming extended sand flats and bars covered with tidal dunes (Fig. 5O). Note that the top of all sand flats in both rivers can be strongly reworked at low tide by wind action, inducing important eolian sand fluxes..

4.3. Sediments grain size, mineralogy and geochemistry

The grain-size distribution curves indicate a variable amount and mixing of three distinct modes that can be detected in most samples (Fig. 7): Medium to coarse silt (MCSi), Very fine to fine sand (FS) and medium sand (MS). The Chico and Santa Cruz Rivers have the same overall grain-size pattern. Along the Chico River, there is a clear seaward coarsening of tidal flat sediments. Such trend is not clear along the Santa Cruz River. As expected, MCSi to FS is the main mode in mud and mixed flats while MS are the main mode in bars, both fluvial and tidal. MCSi is the main mode of eolian sediments preserved on top of the terraces.

All bulk-rock samples show similar composition: quartz, Ca-felspar, zeolite and muscovite, with traces of chlorite. The most abundant element into all samples is Si, that slightly increases with grain-size increase.

XRD analyses of the clay grain-size fraction (Fig. 8) show that most samples are dominated by well-crystallized smectite (from 66% to 93%). Two samples, 2018-9 and 2018-17, corresponding to the aeolian dusts, have up to 45% of illite, are slightly richer in chlorite and contain rutile in the bulk samples. When plotted in a ternary diagram (Fig. 9A), most samples aligned on a mixing line between the smectite and illite+chlorite end-members ranging from 93% (sample 2019-2) to 66% (sample 2019-1) of smectite. The crystallographic parameters (Fig. 9B) of illite indicate that parent-rock of illite were low-grade metamorphic rocks (anchizone to epizone – low pressure and temperature) and that illite is Fe- and Mg-rich.

The spatial distribution of major and trace elements in surface sediments is displayed in Fig.10. Sediments in the Santa Cruz-Chico estuary may originate from any of the surrounding geological provinces at the Southern Patagonian Andes. These potential source areas are characterized by different major or trace-element compositions. Thus, by connecting the major or trace element composition of source areas to the terrigenous particles in the sediment, the origin of the particles can

be identified. In order to characterize the spatial changes in detrital material, different major oxides (SiO2, CaO, K2O, TiO2, Fe2O3, MnO) and trace elements (Sr, Rb, Zr) in different sediment facies (sand to mud flat environments, gravel bars, fluvial sands and eolian dusts) have been measured. In general, results do not evidence significant up- to downstream gradient, either difference between sediment facies (Fig. 10). Sediment samples contain SiO2 (between 50 and 74%, mean value 56%), CaO (0.6 – 2,6%, m.v. 1.9%), Fe2O3 (1.8 – 6.5%, m.v. 4.7%), MnO (0.11 – 0.2%, m.v. 0.08%), TiO2 (0.2 – 0.7%, m.v. 0.6%), Sr (123-322 ppm, m.v. 247 ppm), Rb (55-107 ppm, m.v. 76 ppm), Zr (86-243 ppm, m.v. 160 ppm). Calcimetric analyses (not shown herein), indicate very low values of CaCO3, below 1% and averaging 0.62%. The eolian dusts (Samples 09, 10, 17) show similar geochemical signature, and an higher-than-average values in S.

4.4. Meiofauna

Over the 22 samples analyzed for meiofauna, 1084 specimen of foraminifera and testate amoebae were observed, distributed within 24 species, 18 of foraminifera (F) and 6 of testate amoebae (TA) (Table S1, Figs. 11, 12).

All species are agglutinated excepted *Buliminella elegantissima* (F) that is hyaline (only one single specimen in sample SC2023-1). The density ranges from no meiofauna (6 samples) to 1125 specimens for an equivalent of 100 cm^3 of sediments. The most common species are *Remaneica plicata* (F), *Lepidodeuterramina eddystonensis* (F) and *Entzia macrescens* (F). The distribution of density and species is not homogeneous in the estuary. The highest densities are towards the mouth of the estuary and the lowest densities are upstream. The highest proportion of testate amoebae occurs in the sample SC2019-02, the most upstream sample collected in the Santa Cruz River (Fig. 11). The second sample with highest proportion of testate amoebae, SC2023-5, is located on the SW side of the intermediate basin, at equal distance between the confluence and the outlet. SC2023-5 is the uppermost sample of a local cross-shore transect, collected on a levee isolating the sediments from daily marine influence (Fig. 11). The other samples are dominated by foraminifera. *Remaneica plicata* and *Cribrostomoides jeffresyii* are dominant in samples from the intermediate basin and confluence, whereas *Lepidodeuterammina* species and *Entzia macresens are present* upstream (Fig. 11).

4.5. Seismic data

In spite of their relatively poor quality and of their reduced length with respect to the estuary size, seismic lines shot into the intermediate basin provide some valuable information on the sediment infill of this area.

Three main units can be distinguished above the rocky substrate (Fig. 13):

A basal unit (U1), resting on the substrate through a more or less irregular basal surface of generally low amplitude. It shows a lenticular geometry with positive relief up to 10 m high, and 1-2 km long. Almost no internal reflectors are visible on the seismic data, indicating that penetration is poor, probably in relation to the very coarse-grained nature of the sediment (gravels, pebbles). When visible, internal reflectors are either conformable to or truncated by the basal surface of U2.

The second unit (U2) constitutes the main volume of the infill. It rests on U1 and on the substrate. Its thickness reaches up to 10 m. It contains generally chaotic seismic facies. Locally, reflectors with channelized shapes are visible. Penetration of the seismic signal is variable within U2, and seismic facies range from very low to very high amplitude. This may reflect lateral and vertical changes in sediment nature, probably from gravels to sands. The basal surface of U2 is mainly erosional.

The third unit (U3) is a sediment cover, a few meters thick, shaped by subaqueous dunes. Its topography generally draws bank-shaped bodies. U3 rests on U2 as well as on U1, locally directly on the substrate (this last feature is not seen on the seismic profile in Fig. 13, but it is observed directly on the field), through a surface that is mainly erosional. The orientation of the dune on top of U3 is hardly discernible on the available seismic lines. Most dunes appear symmetric, locally with a rounded shape. In some places, flood tidal current-oriented dunes can be distinguished. Seismic line orientation is clearly not suitable for the dune asymmetry to be detected. Moreover, since the lines were shot at high tide, i.e. after a stage of flood tidal current, the occurrence of flood-oriented dunes is logical.

Very locally, transparent seismic facies form reflection masks with abrupt vertical side limits. This could be due to gas trapped inside the infill, which would imply that impermeable (clayey? highly compacted?) layers are preserved in the later.

4.6. GPR data

From the GPR data collected into the gravel barrier system of the estuary mouth, the following main features have been highlighted (Fig. 14):

Most GPR lines show a regular progradational pattern of construction.

The height of the beachface in the gravel beach ridges commonly exceeds the GPR penetration depth (6 m).

The successive beachfaces that prograde do not show drastic changes in slope that could indicate strong erosion or scour processes.

On the northern side of the mouth, beach ridges and spits form distinct terraces of decreasing altitude seaward from 11 m to 8 m amsl, separated from each other by fine-grained low flats (Fig. 5D, Fig. 14A). On the southern side, beach ridges form a more amalgamated system (Fig. 5C), but also with a clear stair-case seaward decrease of altitude of successive beach ridge packages from 8.6 to 5.5 m amsl (Fig. 14B).

5. Discussion

5.1. Sediment sources

At a general scale, the mineralogical and geochemical analysis of bulk samples are consistent with a terrigenous/volcaniclastic signature mainly derived from erosion of various lithologies of rocks exposed in the Patagonian Andes and central Patagonia, to the west of the studied area. These lithologies are also reflected by the composition of pebbles in the fluvial terraces of the Santa Cruz and Chico rivers (Oblak, 2021), dominated by quartzites and metasedimentary rocks of the Bahía La Lancha and Río Lácteo Formations (Late Devonian – Early Carboniferous) and volcanics of the Complejo El Quemado (Middle Jurassic). The geochemical data show a certain homogeneity among the different samples. This is consistent with the conclusions of Gaiero et al., (2007) who analyzed riverbed and suspended sediment samples from different Patagonian rivers, topsoil samples across the Patagonian tableland, and eolian dust samples along the coast (from 39°S to 52°S). The geochemical analyses of the samples

conducted in the region of the Santa Cruz and Chico rivers are consistent with the present study measurements (Table S2): SiO2 (between 50 and 66%), CaO (2.5–4.2%), Fe2O3 (4.7–5.9%), MnO (0.09–0.15%), TiO2 (0.79–3.63%), K2O (1,38 – 2,05%, m.v. 1,71), Sr (241–349 ppm), Rb (39–72 ppm), Zr (153–303 ppm). All these samples exhibit a homogeneous geochemical signature and result from a mixture of material from the southern volcanic zone (SSVZ) and Jurassic rhyolites (Gaiero et al., 2007). Fine-grained, unconsolidated Miocene sediments of epiclastic and volcaniclastic composition are also extensively exposed in the central part of Patagonia. In addition, Quaternary fallout deposits of explosive volcanism are widespreaded all over the Santa Cruz province and the South Atlantic Ocean (Scasso et al.,1994; Gaiero et al. 2007; Kratzmann et al., 2010). Fragments of all these lithologies were combined to produce these Si and Al rich, immature sediments with unstable minerals like augite, product of negligible weathering in Pliocene-Recent times because of the desertic Patagonian climate. Non-carbonate Ca occurrence must reflect high amount of plagioclase from the paleo- and neovolcanic sources mentioned above. This is supported by the presence of abundant Ca-felspars associated to zeolite in the bulk samples as revealed by XRD spectrums (Fig. 8). Although grain-size control on the geochemistry of the sediments does not seem to be strong (Fig. 10B), higher content of physils in the slightly finer-grained sediment of the Chico River samples results in higher Al content. On the contrary coarser-grained sediments are slightly enriched in Si.

The mineralogy of the clay grain-size fraction displays a classic terrigenous/volcaniclastic signature (Fig. 8). Dominant smectite in the fraction <2µm suggest unconsolidated, volcaniclastic Miocene sediments together with glass-rich, primary or reworked fallout deposits, as important detrital sources. Together with abundant zeolites in the bulk samples, this suggests a volcaniclastic contribution because these minerals are common products of weathering and alteration of unstable volcanic particles (Chamley, 1989). Weathering of Miocene volcaniclastic sediments occurred previous to Pliocene times and alteration of recent, glassy, fallout deposits is easier in soils of humid areas of the Cordillera Patagónica (Petschick et al., 1996; Diekmann et al., 2000). The similar smectite content in the Santa Cruz and Chico rivers and the local, upstream increase of smectite in the fraction <2µm, with maximum smectite concentration in the most upstream sample collected and reduced concentration at the outlet of the rivers, also suggest a remote source for smectite. The crystallographic parameters (Fig. 9B) of

illite indicate illite provenance from the Devonian, low-grade metamorphic rocks of the Río Lácteo/Bahía la Lancha Formations (Fig. 1B).

The two samples dominated by illite in the fraction <2µm correspond to MCSi eolian deposits (samples 9, 17) at the margins of the Chico and Santa Cruz rivers. As smectite is also dominant in some other MCSi samples as well as in both, finer- and coarser-grained fluvial or tidal facies, this must be the result of different sediment sources and not a grain-size bias. Therefore, a distinct, specific provenance for the eolian particles is possible. Clay suites incorporated in aeolian, glacial, and fluvial deposits mostly reflect their detrital sources (Chamley, 1989). However, the decreasing influence of local sources with increasing distance of transportation and with the increased importance of wind storms that homogenize the products of different sources and cause severe sorting, is noted by Chamley (1989) as well. As a consequence, the most widespread and resistant minerals, like mica-illite and quartz, tend to be more abundant and more widely distributed (Chamley, 1989). Long-distance transport by wind or, more likely, wind storms, may have sorted out illite preferentially in the case of the SC-CR eolian sediments. At last, the higher-than-average values in S in the eolian samples can be explained by their possible organic matter component due to very fine-grained plant debris originating from local bush vegetation and soils.

5.2. Fluvial to marine transition depicted by meiofauna

Foraminifera and testate amoebae can be used to delimitate marine from continental freshwater environments (Charman, 2001; Leipnitz et al., 2014; Armynot du Châtelet et al., 2018). All the studied samples of the SC-CR estuary can be considered as transitional between brackish and freshwater environments. The SC-CR foraminifera assemblage, dominated by agglutinated shells, is typical of environments influenced by continental freshwater supply, or associated with low pH salt marshes, avoiding calcium carbonate bearing shell foraminifera to develop (Murray, 2006). No hyaline foraminifera have been found that would account for a direct supply of marine sediment. Most of the testate amoebae observed in the SC-RC samples live in a variety of freshwater environments ranging from arid deserts to rainforests (e.g., Smith et al., 2008; Fernandez, 2015). By comparison to the closest study from Tierra del Fuego (Caffau et al., 2015), the testate amoebae diversity is equivalent but remains low by comparison to most of the southern hemisphere studies that describe testate amoebae

(e.g., Bonnet, 1981; Smith and Wilkinson, 1986; Smith 1992; Vincke et al., 2006; Smith et al., 2008; Heger et al., 2009; Mieczan and Adamczuk, 2015; Bamforth, 2014; Whittle, 2019). Thanks to the clear difference of proportions of foraminifera vs testate amoebae (Fig. 15), the landward extent of the salt wedge in the Rio Santa Cruz is delineated by samples 2023-23/24/26/29 (Fig. 11; Table S1). Samples 2018-2/6/11 undergo a large brackish influence and 2019-2 sample, upstream of Cmdt Luis Piedrabuena, is fully fluvial. In the Chico River, the most upstream sample (SC2018-06) is under marine influence with brackish and typical tidal flat species. Therefore, the salt wedge limit is still to be found in the Chico River. Sample SC2023-5, much richer in testate amoebae, and to a less extend sample SC2023-03 (Fig. 11; Table S1), both located on the SW side of the intermediate basin, evidence the influence of freshwater supplied from the top of the intertidal zones. The same occurs for sample SC2018-02 located at the Chico River mouth.

5.3. Sediment dynamics and depositional environment distribution

According to our observations of facies and morphosedimentary features together with sediment characteristics as well as available data such as those from discharge measurements, the SC-CR estuary can be defined as a composite system (Fig. 16). The complexity mainly reflects differences in fluvial and tidal dynamics into the three main compartments, the Santa Cruz and Chico rivers, and the intermediate basin, as well as differences in sediment and water discharge by the two rivers, and wave action.

The Santa Cruz River water discharge is considerably much larger than that of the Chico River. Sediment supply by the Santa Cruz is consequently larger but mainly as sand/gravel bedload discharge. Fine-grained suspended sediment supplied by the Chico River is 10 times higher than that supplied by the Santa Cruz (Ezcurra and Schmidt, 2018; Schmidt et al., 2018). Due to tidal dynamics, part of the fine-grained sediment supplied by the Chico River is assumed to be redistributed into the downstream part of the Santa Cruz River, contributing to the aggradation of mud flats. On the other hand, the sand supplied by the Santa Cruz River is partly stored into extended sand flats at its mouth, as well as at the confluence and within the downstream part of the Chico River under the action of tidal currents. Sand from the Santa Cruz contributes as well to the development of an elongated banner-like sand flat at the

junction with the intermediate basin. On the other side of the upstream part of the intermediate basin, at the junction with the Chico River, a very large elongated mixed flat develops due to the dual sand and clayey sediment supplies from the Santa Cruz and the Chico rivers. Elsewhere within the intermediate basin, sand and gravel form elongated bar chains, whereas finer-grained sediments accumulate as flats in between the bars. Some of the elongated sand and gravel bars form levee-like bodies parallel to the main subtidal channels. Along the Santa Cruz River down to the outlet, the Miocene bedrock is sparsely exposed at the lower fringe of the intertidal domain (cf. Fig. 5G), suggesting that the river channel and the intermediate basin are mostly sediment by-pass areas. South from Puerto Santa Cruz, erosional features (including erosion of present and former mudflats as reflected by the development of shore-normal furrows) progressively take over deposition along the shores, down to the gravel beachridges of the mouth area. The only significant sediment bodies in the intermediate basin are fan deltas formed at the outlet of tributaries incised across the Miocene cliffs forming the southern shore of the basin. The triangular-shaped deltas are mostly composed by accretion of gravel beach ridges formed at the mouth of the small feeding rivers. This supports the idea that waves influence the shores of the intermediate basin.

From this overall morphosedimentary interpretation of the SC-CR estuary (Fig. 16), it can be suggested that the Santa Cruz River arm is mainly fluvial-dominated, while the Chico River arm is tide-dominated. These conclusions are also supported by the meiofauna distribution, showing a much larger extent of brackish waters upstream the Chico River, and by the damping of the tide and occurrence of only freshwater species a short distance upstream Comandante Luis Piedra Buena in the Santa Cruz. Only the downstream part of the Santa Cruz River can be considered as tide-influenced and, together with the confluence area, is where a maximum of fine-grained (i.e., not gravels) sediments is stored. This sedimentation area could be assimilated to a bayhead “delta” (to oppose it to open-ocean delta), resulting in considering the whole system as resembling to a wave-dominated estuary (Dalrymple et al., 1992). However, the intermediate basin is far from being the lowest tidal energy domain of the system, and consequently it is not comparable to the central basin of wave-dominated estuaries. On the other side, the Chico River arm displays the main characteristics of a tide-dominated estuary, with a single sinuous fluvio-tidal channel upstream evolving downstream towards a more complex braided or anastomosed system, ending towards the mouth (confluence) with more elongated bars.

Due to the narrowness of the outlet with respect to the intermediate basin size, and to its important water depth, both contributing to generate powerful ebb tidal currents, it is likely that only a very minor part of the fine-grained sediments (muds to sands) supplied by the two rivers is preserved in the intermediate basin defined previously as a by-pass area. The scattered dunes identified on seismic data in the subtidal channels of this basin mostly correspond to lag bedforms flooring the scoured Miocene bedrock or older Holocene deposits, which emerge at the Leones Island. The bypass of sand and mud probably explains the morphological stability of the basin shoreline at a centennial scale. Most of the sand and fine-grained sediment is exported offshore, as evidenced by plumes (Fig. 16), probably settling to form a large subaqueous shelf delta (Fig. S1). Such sediment by-pass is consistent with ria-type or rock-bounded estuaries, and probably enhanced during sustained high water discharge periods (as explained by Fitzgerald et al., 2000; 2002 in the case of rock-bound, mesotidal riverine-associated tidal inlets along the USA northeastern coast), or by the interplay of strong westerly winds that reinforce river and ebb tidal currents (Piccolo and Perillo, 1997).

The meltwater surges in the Santa Cruz River, due to the frequent ice dam collapses of the Argentino Lake, can be tentatively considered as the cause of flushing and offshore exportation of sand and mud that could otherwise deposit in the intermediate basin. However, considering a mean tidal range of 5 m over the entire SC-CR system upward, the related tidal prism would be responsible for a water discharge of the order of 50000 m^3s^{-1} (averaged on a half semi-diurnal tidal cycle). This exceeds by far the maximum water discharge related to highest river floods (2500 m^3s^{-1}). As a consequence, the intermediate basin can be considered as a ria-type estuary, and the subaqueous shelf delta an ebb-tidal delta.

Note that Archer (2013), in his synthesis on hypertidal estuaries, described the whole Santa Cruz – Chico River system as a tide-dominated estuary, sensu Dalrymple et al. (1992). Our conclusions show that this model cannot be used. Only the Chico River domain can be considered as a tide-dominated estuary. As a whole, the SC-CR estuary could be described as a hybrid system comprising a tide-dominated estuary (Chico River) and a tide-influenced river mouth, both converging and flowing out into a hypertidal ria-type estuary, the outlet of which is a short and narrow strait featuring an emergent rocky substrate and wave-dominated gravel barriers. This ria-type estuary shares common features with rock-bound estuaries (FitzGerald et al. (2000). The SC-CR estuary, in spite of its complexity due to specific

local factors, related to tide conditions, hydro-climate regime and geological context, can be partly explained using and combining existing models (Dalrymple et al., 1992; FitzGerald et al., 2000). The intermediate basin however has no real counterpart, which points out that models necessarily have some limitations as stated by Dalrymple and Choi (2007). We suggest that such very high energy tidal basins could feature the hypertidal estuaries of south Patagonia, especially the Rios Gallegos estuary, characterized by 12 m tidal range, a rock-bound mouth and an extended ebb-tidal delta (Bindelli et al., 2023).

5.4. Holocene evolution - Sediment infill organization

Field observations, together with seismic reflection and GPR data, help to figure out the stratigraphic organization of the Holocene deposits of the SC-CR estuary and to compare them with well-known counterparts in the Northern Hemisphere (Dalrymple and Zaitlin, 1994; Chaumillon et al., 2010; Tessier, 2012; Tessier et al., 2012). This is also an occasion to consider the impact of sea level changes on the morphology and dynamics of large estuarine systems. While most of Northern Hemisphere large estuaries that have been considered in text-book models have evolved in almost stillstand condition for the last 5 millennia, this is not the case for the SC-CR system. Many works have been conducted along the Patagonian coasts to reconstruct the relative sea level curve during the last post-glacial transgression. The area is subject to a more or less constant uplift, mainly of tectonic origin and in the order of 0.1 mm/y (Rostami et al., 2000; Pedoja et al., 2011). The resulting relative sea level curve displays a rise until a maximum altitude, about 7-8 m amsl at around 7500 y. BP, and then a slow decrease until the present-day level. During that period, Zanchetta et al. (2014) suggested that two important phases of sea level stillstand occurred, around the maximum and around 3500 y.BP, and Sheldman and Radtke (2010) pointed for two periods with more rapid falls at about 6000 y. BP and 2200 y. BP.

GPR data acquired on both sides of the inlet clearly show the regular progradational pattern of construction of the gravel barriers together with their progressive decrease in altitude. This fits with the relative sea-level fall since the maximum Holocene high level. On the northern side, the altitude of the barrier (Fig. 14A) reaches almost 11 m, and about 8 m for the most nearshore one. On the southern

side, altitudes are lower, ranging from about 8-9 m to about 6 m (Fig. 14B). The northern side of the inlet is obviously more exposed to wave action, either induced by the dominant westerlies or by Atlantic storms, explaining that barriers are higher on this side of the inlet. The exposure to wave and storm surges was probably even worse when the inlet was much wider during the Holocene highest sea level. Another difference between the north and south relates with the main arrangement of the barriers. In the south, they form an amalgamated beach ridge system, whereas in the north barrier spits feature successive terraces, more or less discontinuous, separated by extensive tidal flats. The stepped decrease of sea level after *ca.* 7000 BP as suggested by Sheldman and Radtke (2010) and Zanchetta et al. (2014) is probably responsible of the pronounced stepped arrangement of spit terraces in the north. This stepped disposal is not so well expressed into the amalgamated system in the south. We suggest that the difference between both sides of the inlet has been enhanced due to gravel supply, as explained by Montes et al. (2018) along Tierra del Fuego coast, and available space with respect to the underlying substrate and the inlet. Indeed, due to the proximity of the cliff and the erosion of alluvial terraces above, inshore and offshore, gravel supply is very large in the south and barriers have developed along a narrow band between the cliff and the inlet. In the north, sources able to deliver a high amount of gravels were not so proximal, and littoral drift resulted in elongated and fragile spits. As they developed on an extensive and probably flat surface, the system better responded and recorded sea level fall steps.

The seismic data collected in the intermediate basin showed the reduced thickness of the infill, formed by three main sediment units above the Miocene substrate. Although sediment cores are not available to ground-truth seismic line and provide age data, the following hypothesis is proposed, based on regional key-ages of sea level changes (Sheldman and Radtke, 2010; Zanchetta et al., 2014) in addition to information supplied by seismic facies characteristics and seismic unit geometries: the basal unit (U1, Fig. 13) is made of gravel and is interpreted as remnants of lowstand fluvial gravel deposits (Fig. 17). The two units above are thought to be related to the Holocene transgression. When the sea reached its highest level, around 7500 y. BP, leading to the maximum flooding of the ria, and to the widening of the inlet, the larger volume of the tidal prism must have enhanced tidal dynamics. The first transgressive sediments deposited prior to the Holocene maximum, were later reworked by powerful tidal currents. Usually, early transgressive deposits within an incised valley are organic-rich facies, producing gas

once buried (e.g. Tessier et al., 2012). The scarcity of gas on the seismic profiles tends to demonstrate that this was not the case for the SC-CR incised valley, probably due to climatic conditions during the early Holocene. Another hypothesis is that very little of these early transgressive facies has been preserved. The tidal ravinement surface may indeed have deeply cut into the underlying lowstand alluvial deposits and reach locally the substrate (Fig. 17). Such deep erosion by the tidal ravinement surface into macro- to hypertidal incised valleys is commonly described (e.g., Chaumillon et al., 2010; Tessier, 2012). Deep ravinement due to tidal currents is also depicted in the transgressive Holocene infilling succession of the Golfo San Jorge in Central Patagonia (Desiage et al., 2023) and even in Miocene sediments of Patagonia (Scasso and Cuitiño, 2017). When sea level fall started after the maximum Holocene transgression and stillstand, the process of tidal ravinement probably continued, or maybe was enhanced. However, the reduction of the tidal prism induced by the sea level fall led tidal dynamics to decrease progressively, favoring sediment deposition and preservation. The deposition of U2 is thus assumed to be related to this period. Seismic data show that the last unit of infilling, U3, the top of which features the present-day tide-dominated sand and gravel transport, developed above U2 through an erosional surface (Fig. 14). We suggest that this is the modern tidal ravinement surface that marks the very slow sea level fall,or stillstand,of the late Holocene, i.e. around 3500 y. BP. Similarly to U2, U3 could deposit and be preserved after 3500 y. BP, maybe in relation to the last falling stage at about 2200 y. BP, and a consecutive tidal prism reduction. However, U3 covers only partially the tidal ravinement surface that remains highly active at present, erosion and by-passing being the dominant processes at the intermediate basin and inlet bottom.

The characteristics of the Holocene sediment infill into the intermediate basin seems to reflect competing erosional and depositional processes. This opposition fluctuates in time due to relative sea-level fall that induces both water depth decrease, promoting erosion, and tidal prism reduction, promoting sedimentation. Sediment supply, especially from the Santa Cruz River, should be an additional factor that modulates this duality. At the seaward end of the intermediate basin, due to the constant reduction of the inlet width in relation to barrier progradation, tidal current velocities have permanently been very powerful. There, the tidal ravinement is the deepest and it is probably still incising the substrate.

6. Main conclusions and perspectives

Our exploration of the Santa Cruz – Chico River estuary allows exemplifying a large hypertidal estuary in terms of morphosedimentary organization and Holocene infill stratigraphy, highlighting specificities reflecting the combined effect of tidal dynamics and South Patagonian climatic and tectonic conditions.

- The SC-CR estuary can be defined as a hybrid ria-type estuary composed of 4 main domains: a tide-influenced fluvial mouth (the Santa Cruz River) and a tide-dominated estuary (the Chico River), both converging towards an elongated subtidal ria-type estuarine basin; sandy and muddy sediments supplied by the two rivers by-pass this hypertidal basin, and are exported offshore through a narrow outlet, and settle forming an ebb-tidal delta.

- Sediment mineralogy and geochemistry along the estuary do not evidence significant up- to downstream trends in relation to sediment sources and transport dynamics. This is due to the high degree of sediment mixing, and to the highly predominant volcanic nature of sediment sources. Sediment content in meiofauna, represented by agglutinated foraminifera and testate amoeba, is the only tracer that shows significant changes, useful to delimitate upstream salt water intrusion. This limit is located ca 25 km upstream of the Santa Cruz River mouth, while it remains to be found upstream on the Chico River. However, its distance from the Chico River mouth is probably roughly the same as the one on Santa Cruz River.

-Typical tidal environments and facies are mostly developed along the Chico River and at the downstream portion of the Santa Cruz River. They comprise sand flats and tidal dunes, and mixed to mud flats containing tidal rhythmites. Along the subtidal ria-type basin, almost no tidal flats are preserved. In contrast, the gravel beaches present all along the basin, including the gravel beachridges that shape fan deltas developed on the southern side, demonstrate that waves exert a strong action within the hypertidal estuarine basin.

- The sediment infill, pictured by seismic data, reflects relative sea-level evolution and concomitant tidal prism fluctuation during the Holocene. The most prominent surface in the infill is the tidal ravinement surface that formed during the Holocene highstand, at ca 7500 y. BP, when the tidal prism was the

highest. After 7000 y. BP, relative sea level fell, and the infill resulted from a competition between erosion, promoted by water depth decrease, and deposition, favoured by tidal prism reduction. Tidal ravinement occurring during the fall can be defined as a regressive tidal ravinement. Sediment by-passing and erosion of valley-bottom, especially at the outlet, are nowadays the predominant processes. The apparent hugeness of the ebb tidal delta resulting from the offshore sediment export could suggest that these processes have operated for a very long time.

Although our study allows to draw a quite complete morphosedimentary portray of the Santa Cruz-Chico River hypertidal estuary, completing the pioneer descriptions of Archer (2013), and to provide for the first time elements to depict its Holocene infill stratigraphy, many questions remain, opening interesting perspectives for a better understanding of such hybrid systems. For instance, it is suggested that the dynamic of infill is a very complex process depending on the resulting combination between water depth and tidal prism fluctuations, in addition with variations in sediment supply. Numerical modelling is probably the most reliable tool for testing different scenarios. Interestingly it could be used as well to test how tidal range has evolved during the Holocene. Tidal range has been considered to be unchanged in comparison with the present-day conditions, or possibly higher during the Holocene highstand. A significant increase of tidal range since the Holocene highstand has never been hypothesized. The impact of such an increase on the infill dynamic and stratigraphic features would have to be figured out. On the other hand, the geometry, thickness, and composition of the ebb tidal delta, which necessarily feature the evolution of this complex dynamics during the Holocene, remain to be explored. Seismic data would in addition inform whether the ebb-tidal delta body could partly be a geomorphologic heritage of previous low sea-level deltas. Numerical modelling could be used as well to test if the meltwater surges of the Santa Cruz River that occur periodically may account significantly for offshore sediment expulsion. Estimation of the present-day tidal prism argues for concluding that their impact is negligible but this should be numerically tested. This last remark leads to question as well on the future evolution of the estuary and offshore sediment dynamics. Indeed, when the construction of the two dams upstream on the Santa Cruz River will be completed, this will necessarily regulate the river water discharge and thus reduce meltwater surges. A decrease in sediment delivery to the estuary should be as well expected, modifying consequently the tidal flat morphodynamics at the river mouth and confluence area. The impacts on the offshore reaches of the estuary, due to changes

in the extension of the plumes and in their sediment content and concentration, will need to be assessed.

Credit author statement

BT: Conceptualization, funding acquisition (lead), project administration (lead), supervision (lead), Field surveys, data acquisition, processing and interpretation, writing – review & editing. **JYR**: Funding acquisition (lead), project administration, Field surveys, data acquisition, processing and interpretation, writing – review & editing. **JC**: funding acquisition (lead), project administration, supervision, Field surveys, data acquisition, processing and interpretation, writing – review & editing. **RS**: Funding acquisition (lead), project administration (lead), supervision, Field surveys, data acquisition, processing and interpretation, writing – review & editing. **LP**: Field surveys, data acquisition, processing and interpretation, writing – review & editing, **MD**: Field surveys, data acquisition and interpretation, review & editing, **PW**: Data processing and interpretation, review & editing, **VBR**: Data processing and interpretation, review & editing, **EAC**: Data processing and interpretation, review & editing, **AK**: Data processing and interpretation, review & editing, **TL**: Data processing and interpretation, review & editing, **LD**: Data processing and interpretation, review & editing.

Funding

This research on the Santa Cruz-Chico River estuary is part of the project “Hypertide” funded by the ECOS-SUD – MINCYT programme between Argentina and France. Additional funding has been provided by the CNRS-INSU (SYSTER programme) and by the different laboratories involved on the project on their own research funds. PhD grants were received from the French Ministry of Research for Léo Pancrazzi, from the Normandie Region and Direction régionale de l’environnement, de l’aménagement et du logement for Thibaud Lortie, and from the CONICET for Maria Duperron.

Acknowledgments

The authors would like to thank first Nadia Da Silva for the administrative management of the ECOS-SUD – MINCYT project Hypertide. They would like to warmly acknowledge the Prefectura Naval Argentina of Puerto Santa Cruz, and its Major Arnaldo Ramírez who kindly welcomed the team and

gave us permission to use the safety boat of the Prefectura, the crew of which is also greatly thanked, especially Captain Villalba and Captain Britez. The authors are grateful as well to the owners of fields around the estuary who allowed us to get access to the estuarine shores through their private properties. We thank Magalie Legrain (M2C Lab, Caen) for grain-size analyses, and Philippe Recourt (LOG Lab) for XRD analyses (using infrastructure and technical support from the platform CARMIN – University of Lille). The TanDEM-X data were provided by the German Aerospace Center under the scientific project DEM-GEOL1108. The authors are very grateful to Dr. Kyungsik Choi and an anonymous reviewer for their constructive comments and useful reviews, which contributed to improve the manuscript. We also thank Dr. Catherine Chagué, Editor-in-Chief of Sedimentary Geology, for her helpful advice to improve the earliest version of the article. Finally, we would like to dedicate this article to Allen William Archer, who died in August 2022. He was the first tidal sedimentologist to explore this fabulous SC-CR estuary. Our tidal geologist community owes a lot to his free and pioneering spirit.

References

Archer, A. W., 2013. World's highest tides: Hypertidal coastal systems in North America, South America and Europe. Sedimentary Geology 284, 1-25.

Archer, A. W., Hubbard, M. S., 2003. Highest tides of the world. In: Chan, M.A., Archer, A.W. (Eds.), Extreme Depositional Environments: Mega End Members in Geologic Time: Geological Society of America Special Paper 370, 151–173.

Armynot du Châtelet, E., Francescangeli, F., Bouchet, V.M.P., Frontalini, F., 2018. Benthic foraminifera in transitional environments in the English Channel and the southern North Sea: A proxy for regional-scale environmental and paleo-environmental characterisations. Marine Environmental Research 137, 37-48.

Ávila, P., Ávila, M., Dávila, F. M., Ezpeleta, M., Castellano, N. E., 2023. Patagonian landscape modeling during Miocene to Present-day slab window formation. Tectonophysics 229971. DOI: 10.1016/j.tecto.2023.229971

Bamforth, S.S., 2014. Composition of soil testate amoebae communities: Their structure and modifications in the temperate rain forests of New Zealand and Tasmania. The Journal of Eukaryotic Microbiology 62, 217-226.

Berryman, K. R., Ota, Y., Hull, A. G., 1992. Holocene evolution of an estuary on a tectonically rising coast: the Pakarae River locality, eastern North Island, New Zealand. Sedimentary Geology 80(3-4), 151-165.

Beny, F., Bout-Roumazeilles, V., Davies, G.R., Waelbroeck, C., Bory, A., Tribovillard, N., Delattre, M., Abraham, R., 2020. Radiogenic isotopic and clay mineralogical signatures of terrigenous particles as water-mass tracers: New insights into South Atlantic deep circulation during the last termination. Quaternary Science Reviews 228, 106089.

Bindelli, L., Re, M., & Kazimierski, L. D.,2023. Hydrokinetic energy potential in Argentine estuaries with high tidal ranges. IEEE Latin America Transactions 21(9), 1049-1055.

Bonnet, L., 1981. Thécamoebiens (Rhizipoda testacea). Bulletin du Comité National Français de Recherches Antarctiques 48, 23-32 (in French).

Brindley, G.W. and Brown, G., 1980. X-Ray Diffraction Procedures for Clay Mineral Identification. In: Brindley, G.W. and Brown, G., Eds., Crystal Structures of Clay Minerals and Their X-Ray Identification, Mineralogical Society 305-356. DOI : 10.1180/mono-5.5

Caffau, M., Lenaz, D., Lodolo, E., Zecchin, M., Comici, C., Tassone, A., 2015. First evidence of testate amoebae in Lago Fagnano (54°S), Tierra del Fuego (Argentina): Proxies to reconstruct environmental changes. Journal of South American Earth Sciences 64, 27-41.

Castaing, P., Guilcher, A., 1995. Geomorphology and sedimentology of rias. In: Perillo G.M.E. (Ed.) Geomorphology and sedimentology of estuaries. Developments in Sedimentology 53, 69-111. Elsevier.

Chamley, H., 1989. Clay sedimentology. Springer-Verlag, Berlin-Heidelberg. 623 pp.

Charman, D.J., 2001. Biostratigraphic and palaeoenvironmental applications of testate amoebae. Quaternary Science Reviews 20, 1753–1764.

Chaumillon, E., Tessier, B., Reynaud, J. Y., 2010. Stratigraphic records and variability of incised valleys and estuaries along French coasts. Bulletin de la Société géologique de France 181(2), 75-85.

Cuitiño, J. I., Fernicola, J. C., Kohn, M. J., Trayler, R., Naipauer, M., Bargo, M. S., Kay, R.F., Vizcaíno, S. F., 2016. U-Pb geochronology of the Santa Cruz Formation (early Miocene) at the Río Bote and Río Santa Cruz (southernmost Patagonia, Argentina): Implications for the correlation of fossil vertebrate localities. Journal of South American Earth Sciences 70, 198-210.

Cuitiño, J. I., Varela, A. N., Ghiglione, M. C., Richiano, S., Poiré, D. G., 2019. The Austral-Magallanes Basin (southern Patagonia): a synthesis of its stratigraphy and evolution. Latin American journal of sedimentology and basin analysis 26(2), 155-166.

Cuitiño, J.I., Tessier, B., Reynaud, J.Y., Scasso, R.A., Pancrazzi, L. Richiano, S.M., 2023, Intertidal flat sedimentation in the hypertidal Santa Cruz – Chico River estuary, Southern Patagonia: Origins of cyclicities. XVIII Reunion Argentina de Sedimentologia, IX Congreso Latinoamericano de Sedimentologia, Abstracts book, p. 107.

Dalrymple, R. W., Zaitlin, B. A., 1994. High- resolution sequence stratigraphy of a complex, incised valley succession, Cobequid Bay—Salmon River estuary, Bay of Fundy, Canada. Sedimentology 41(6), 1069-1091.

Dalrymple, R. W., Choi, K., 2007. Morphologic and facies trends through the fluvial–marine transition in tide-dominated depositional systems: a schematic framework for environmental and sequence-stratigraphic interpretation. Earth-Science Reviews, 81(3-4), 135-174.

Dalrymple, R. W., Zaitlin, B. A., Boyd, R., 1992. Estuarine facies models; conceptual basis and stratigraphic implications. Journal of Sedimentary Research *62*(6), 1130-1146.

Depetris, P. J., Gaiero, D. M., Probst, J. L., Hartmann, J., Kempe, S., 2005. Biogeochemical output and typology of rivers draining Patagonia's Atlantic seaboard. Journal of Coastal Research 21(4), 835-844.

Desiage, P. A., St- Onge, G., Duchesne, M. J., Montero- Serrano, J. C., Haller, M. J., 2023. Late Pleistocene and Holocene transgression inferred from the sediments of the Gulf of San Jorge, central Patagonia, Argentina. Journal of Quaternary Science 38(5), 629-646.

Diekmann, B., Kuhn, G., Rachold, V., Abelmann, A., Brathauer, U., Fütterer, D. K., Gersonde, R., Grobe, H., 2000. Terrigenous sediment supply in the Scotia Sea (Southern Ocean): response to Late Quaternary ice dynamics in Patagonia and on the Antarctic Peninsula. Palaeogeography, Palaeoclimatology, Palaeoecology 162(3-4), 357-387.

Esquevin, J., 1969. Influence de la composition chimique des illites sur leur cristallinité. Bulletin du Centre de Recherches Pau-SNPA *3*(1), 147 (in French)

Ezcurra, H., Schmidt, S., 2018. Concentraciones de sedimentos en suspensión, niveles del mar, temperatura y salinidad en el estuario del Rio Santa Cruz para distintas condiciones de erogación

de las represas. Informe final, 123 p. ENARSA, https://observatorio.energia-argentina.com.ar/mediateca.php?mode=-1&s=OA06 (in Spanish)

Fernandez, L.D., Lara, E., Mitchell, E.A.D., 2015. Checklist, diversity and distribution of testate amoebae in Chile. European Journal of Protistology 51, 409–424.

FitzGerald, D.M., Buynevich, I.V., Fenster, M.S., McKinlay, P.A., 2000. Sand circulation at the mouth of a rock-bound, tide-dominated estuary. Sedimentary Geology 131, 25 – 49.

FitzGerald, D. M., Buynevich, I. V., Davis Jr, R. A., Fenster, M. S., 2002. New England tidal inlets with special reference to riverine-associated inlet systems. Geomorphology 48(1-3), 179-208.Gaiero, D. M., Probst, J. L., Depetris, P. J., Bidart, S. M., Leleyter, L., 2003. Iron and other transition metals in Patagonian riverborne and windborne materials: geochemical control and transport to the southern South Atlantic Ocean. Geochimica et Cosmochimica Act*a* 67(19), 3603-3623.

Gaiero, D. M., Brunet, F., Probst, J. L., Depetris, P. J., 2007. A uniform isotopic and chemical signature of dust exported from Patagonia: Rock sources and occurrence in southern environments. Chemical Geology *238*(1-2), 107-120.

Ghiglione, M.C., Ramos, V.A. Cuitiño, J.I. and Varberón, V. 2016. Growth of the Southern Patagonian Andes (46–53°S) and Their Relation to Subduction Processes. In: A. Folguera, M. Naipauer, L. Sagripanti, M. Ghiglione, D. Orts and L. Giambiagi (Eds.), Growth of the Southern Andes. Springer Earth System Sciences, Springer International Publishing, Switzerland. DOI: 10.1007/978-3-319-23060-3_10.

Goudie, A., 2018. Rias: Global distribution and causes. Earth-Science Reviews 177, 425-435.

Hayward, B. W., Coze, F. L., Vandepitte, L., Vanhoorne, B., 2020. Foraminifera in the world register of marine species (worms) taxonomic database. Journal of Foraminiferal Research 50(3), 291-300.

Heger, T.J., Mitchell, E.A.D., Ledeganck, P., Vincke, S., Van de Vijver, B., Beyens, L., 2009. The curse of taxonomic uncertainty in biogeographical studies of free-living terrestrial protists: a case study of testate amoebae from Amsterdam Island. Journal of Biogeography 36, 1551–1560.

Kratzmann, D., Carey, S., Fero, J., Scasso, R.A., Naranjo J.-A., 2010. Simulations of tephra dispersal from the 1991 explosive eruptions of Hudson volcano, Chile. Journal of Volcanology and Geothermal Research 190, 337-352.

Leipnitz, I.I., Ferreira, F., Jardim Leão, C., Armynot du Châtelet, E., Frontalini, F., 2014. Foraminiferal and testate amoeba diversity, distribution and ecology in transitional environments of the Tramandaí Basin (Rio Grande do Sul, South Brazil). Marine Biodiversity 44, 415–434.

Lortie, T., Cuitiño, J.I., Tessier, B., Reynaud, J.Y., Roberto Adrián Scasso, R.A., Richiano, S.M., Pancrazzi, L., Condomines, M., Dezileau, L., Lekander, M., 2024, Rhythmites preserved into intertidal flat successions of the hypertidal Santa Cruz – Chico River estuary (Southern Patagonia, Argentina). *IAS 2024*, Aberdeen (Scotland, UK). Available on: https://hal.science/hal-04654564

Martinez, O. A., Kutschker, A., 2011. The 'Rodados Patagónicos' (Patagonian shingle formation) of eastern Patagonia: environmental conditions of gravel sedimentation. Biological Journal of the Linnean Society 103(2), 336-345.

Mieczan, T., Adamczuk, M., 2015. Ecology of testate amoebae (Protists) in mosses: distribution and relation of species assemblages with environmental parameters (King George Island, Antarctica). Polar Biology 38, 221–230.

Montes, A., Bujalesky, G. G., Paredes, J. M., 2018. Geomorphology and internal architecture of Holocene sandy-gravel beach ridge plain and barrier spits at Río Chico area, Tierra del Fuego, Argentina. Journal of South American Earth Sciences 84, 172-183.

Murray, J.W., 2006. Ecology and Applications of Benthic Foraminifera. Cambridge University Press, New York, 426 p. DOI: 10.1007/s10933-007-9190-2

Nelson, A. R., Kashima, K., Bradley, L. A., 2009. Fragmentary evidence of great-earthquake subsidence during Holocene emergence, Valdivia Estuary, south central Chile. Bulletin of the Seismological Society of America 99(1), 71-86.

Oblak, M. 2021. Geología y geomorfología de la zona aledaña al estuario Santa Cruz (SE de la provincia de Santa Cruz). Trabajo Final de Licenciatura, Universidad de Buenos Aires. Unpublished. 134 pp (in Spanish).

Ogden, C.G., Hedley, R.H., 1980. An atlas of freshwater testate amoebae. British Museum (Natural History), Oxford University Press, Oxford, London, Glasgow, 228p

Pancrazzi, L., 2022. Dynamics and internal structure of sand-and-gravel coastal barriers in hypertidal environments: experimental and in-situ approaches. Doctoral dissertation, University of Caen, 235 p. (in French).

Pancrazzi, L., Tessier, B., Weill, P., Mouazé, D., Cuitiño J.I., Reynaud, J.Y., Duperron, M., Scasso, R.A., accepted, Architectures and dynamics of a late Quaternary coarse-grained barrier complex at the inlet of a hypertidal estuary (South Patagonia, Argentina). Journal of South America Earth Sciences.

Parras, A.M., Cuitiño, J.I., 2018. The stratigraphic and paleoenvironmental significance of the regressive Monte Observación Member, early Miocene of the Austral-Magallanes Basin, Patagonia. Latin American Journal of Sedimentology and Basin Analysis 25, 93-115.

Pasquini A.I., Depetris P.J., 2011. Southern Patagonia's Perito Moreno Glacier, Lake Argentino, and Santa Cruz River hydrological system: An overview. Journal of Hydrology 405, 48-56.

Pedoja, K., Regard, V., Husson, L., Martinod, J., Guillaume, B., Fucks, E., Iglesias, M., Weill, P., 2011. Uplift of Quaternary shorelines in eastern Patagonia: Darwin revisited. Geomorphology *127*(3-4), 121-142.

Piccolo, M. C., Perillo, G. M., 1997. Geomorfología e hidrografía de los estuarios. In: Boschi E.E. (Ed.), El mar argentino y sus recursos pesqueros, Tomo 1: Antecedentes históricos de las exploraciones en el mar y las características ambientales, 133-161 (in Spanish).

Piccolo, M.C., Perillo, G.M.E., 1999. The Argentina estuaries: a review. In: Perillo, G.M.E., Piccolo, M.C., Pino-Quivira, M. (Eds.), Estuaries of South America; Their Geomorphology and Dynamics. Springer-Verlag, New York, pp. 101–132. DOI: 10.1007/978-3-642-60131-6_6

Petschick, R., Kuhn, G., Gingele, F., 1996. Clay mineral distribution in surface sediments of the South Atlantic: sources, transport, and relation to oceanography. Marine Geology 130, 203-209.

Prospero, J. M., Ginoux, P., Torres, O., Nicholson, S. E., Gill, T. E., 2002. Environmental characterization of global sources of atmospheric soil dust identified with the Nimbus 7 Total Ozone Mapping Spectrometer (TOMS) absorbing aerosol product. Reviews of geophysics 40(1), 2-1.

Plattner, A. M., 2020. GPRPy: Open-source ground-penetrating radar processing and visualization software. The Leading Edge 39(5), 332-337.

Rostami, K., Peltier, W. R., Mangini, A., 2000. Quaternary marine terraces, sea-level changes and uplift history of Patagonia, Argentina: comparisons with predictions of the ICE-4G (VM2) model of the global process of glacial isostatic adjustment. Quaternary Science Reviews 19(14-15), 1495-1525.

Rutter, N., Schnack, E. J., del Rio, J., Fasano, J. L., Isla, F. I., Radtke, U., 1989. Correlation and dating of Quaternary littoral zones along the Patagonian coast, Argentina. Quaternary Science Reviews 8(3), 213-234.

Sacomani, L. E., Panza, J. L. A., Pezzuchi, H. D., Parisi, C., Pichersky, G., Franchi, M., 2012. Hojas Geológicas 5169-I Puerto Coig y 5169-II Puerto Santa Cruz, provincia de Santa Cruz. Boletín del Instituto de Geología y Recursos Minerales, Servicio Geológico Minero Argentino 392, 1-133 (in Spanish).

Sakai, T., Fujiwara, O., Kamataki, T., 2006. Incised-valley-fill succession affected by rapid tectonic uplifts: An example from the uppermost Pleistocene to Holocene of the Isumi River lowland, central Boso Peninsula, Japan. Sedimentary Geology 185(1-2), 21-39.

Scasso, R.A., Cuitiño, J.I. 2017. The effect of tidal ravinement during transgressive infill of incised valleys in the Miocene Puerto Madryn Formation (Patagonia, Argentina). Geo-Marine Letters 37(4), 427–440..

Scasso, R.A., Corbella, H., Tiberi, P., 1994. Sedimentological analysis of the tephra from the August 12-15, 1991 eruption of the Hudson Volcano. Bulletin of Volcanology 56, 121-132

Schellmann, G., Radtke, U., 2010. Timing and magnitude of Holocene sea- level changes along the middle and south Patagonian Atlantic coast derived from beach ridge systems, littoral terraces and valley- mouth terraces. Earth- Science Review 103, 1–30.

Schmidt, S., Ezcurra, H., Danieli, G., Gramaglia, M., Ezcurra, P., 2018. Modelación hidrodinamica, dispersión y transporte de sedimentos en el estuario del Rio Santa Cruz. In: Serman y Associados S.A., Estudio de impacto ambiental aprovechamientos hidroeléctricos del Rio Santa Cruz, Provincia Santa Cruz. 53 p. (in Spanish).

Scott, D.B., Medioli, F.S., Schafer, C.T., 2001. Monitoring in coastal environments using foraminifera and thecamoebian indicators. Cambridge University Press, New York.

Servicio Geológico Minero Argentino: https://sigam.segemar.gov.ar/visor/

Servicio de Hidrografía Naval: http://www.hidro.gov.ar

Smith, H.G., Bobrov, A., Lara, E., 2008. Diversity and biogeography of testate amoebae. Biodiversity and Conservation 17, 329-343.

Smith, H.G., Wilkinson, D.M., 1986. Biogeography of testate rhizopods in the southern temperate and Antarctic zones, Colloque du les écosystèmes terrestres subantarctiques. CNFRA, Paimpont, pp. 83-96.

Smith, H.G., 1992. Distribution and ecology of the testate rhizopod fauna of the continental Antarctic zone. Polar Biology 12, 629–634.

Tessier, B., 2012. Stratigraphy of tide-dominated estuaries. In: Davis Jr., R., Dalrymple, R. (eds) Principles of Tidal Sedimentology. Springer, Dordrecht, pp. 109-128, Dordrecht: Springer Netherlands. DOI: 10.1007/978-94-007-0123-6_6

Tessier, B., Billeaud, I., Sorrel, P., Delsinne, N., Lesueur, P., 2012. Infilling stratigraphy of macrotidal tide-dominated estuaries. Controlling mechanisms: Sea-level fluctuations, bedrock morphology, sediment supply and climate changes (The examples of the Seine estuary and the Mont-Saint-Michel Bay, English Channel, NW France). Sedimentary Geology 279, 62-73.

Tessier, B., 2023. Tidal rhythmites: Their contribution to the characterization of tidal dynamics and environments. In: M. Green, J.C. Duarte *(Eds) A Journey Through Tides,* Elsevier, pp. 283-305. DOI: 10.1016/B978-0-323-90851-1.00015-7.

Vincke, S., Van de Vijver, B., Nijs, I., Beyens, L., 2006. Changes in the Testacean Community Structure Along Small Soil Profiles. Acta Protozoologica 45, 395–406.

Whittle, A., Amesbury, M.J., Charman, D.J., Hodgson, D.J., Perren, B.B., Roberts, S.J., Gallego-Sala, A.V., 2019. Salt-Enrichment Impact on Biomass Production in a Natural Population of Peatland Dwelling Arcellinida and Euglyphida (Testate Amoebae). Microbial Ecology 78, 534–538.

Zanchetta, G., Bini, M., Isola, I., Pappalardo, M., Ribolini, A., Consoloni, I., Boretto, G., Fucks, E., Ragaini, L., Terrasi, F., 2014. Middle-to late-Holocene relative sea-level changes at Puerto Deseado (Patagonia, Argentina). The Holocene *24*(3), 307-317.

Table and Figure captions

Figure 1. General presentation of the Santa Cruz – Chico River estuary. (A) Location in Southern Patagonia, Argentina; (B) Geological map of the Santa Cruz Province. Data source: Servicio Geológico Minero Argentino (https://sigam.segemar.gov.ar/visor/); (C) Satellite image of the Santa Cruz – Chico River estuary (Sentinel image Sept.1, 2022). CLPD: Comandante Luis Piedrabuena, PSCz: Puerto Santa Cruz, PQ: Punta Quilla, Li: Leones Island, Fg: el Frigorifico. NR3: National Road 3

Figure 2. Digital Terrain Model of the Santa Cruz – Chico estuary area (Data Source: TanDem-X Satellite, German Aerospace Center)

Figure 3. Location of the seismic (A) and GPR (B) profiles acquired in the Santa Cruz – Chico estuary (background on A: Sentinel image May 5, 2022; on B: DTM from IGN 2015 Photogrammetry survey). Note in B that additional GPR data were acquired very recently (February 2023). North arrow for (A) and (B).

Figure 4. (A, B, C) General evolution of the intermediate basin water depth and morphology of the Santa Cruz – Chico River estuary since 1866. (A) Close view on the Estuary extracted from the 1866 map; (B) Nautical map from 1945 (5th edition, 1948). bmsl: below mean-sea level; (C) The most recent Digital Elevation Model available for the area (Ezcurra and Schmidt, 2018; Schmidt et al., 2018); (D, E) Recent morphological evolution of the innermost parts of the system. (D) the oldest available satellite image (1970, Google Earth); (D) the present-day situation (September 2022, Sentinel image). North up on all figures.

Figure 5. Photographs of sub-environments composing the Santa-Cruz-Chico River estuary. (A) Location of the photographs from B to P, with indication of shooting orientation (open eye). (B) Present-day gravel beach from the northern side of the inlet gravel barrier system. Background: Miocene cliffs at the southern side of the inlet area; (C) Gravel beach ridges of the southern side of the inlet gravel barrier system; (D) Isolated gravel ridges encased between two inactive tidal plains in the northern side

of the inlet gravel barrier system; (E) Uppermost gravel beach on top of a mud flat and salt marsh succession along the southern side of the intermediate basin, between Puerto Santa Cruz and Punta Quilla. Salt marsh plants are almost exclusively represented by salicornia. Background: Miocene cliffs at the southern side of the inlet area; (F) Erosional furrows, probably due to wave action combined with ebb-tide runoff, dissecting mudflats close to Punta Quilla; (G) Miocene substrate (highly fossiliferous – thick-shelled oysters - sandy marls) incised by the Santa Cruz River channel; (H) Fluvial (tide-influenced?) terrace incised by the Santa Cruz River channel; (I) Fluvial gravel bars in the Santa Cruz River. Picture taken from the Cmte. Luis Piedrabuena Bridge; (J) Tidal flats and overlying marsh of the internal part of the Chico River; (K) Tidal mud flat at the mouth of the Chico River (Frigorifico locality); (L) Sand flat and ebb-oriented tidal dunes at the mouth of the Chico River; (M) Tidal mud flat upstream of the Santa Cruz River mouth; (N) Tidal sand flat, in cross-shore continuity of (M), along the northern side of the Santa Cruz River; (O) View on the extensive tidal sand flats at the confluence area; (P) The fluvial (tide-influenced?) terrace draped by aeolian silty dust along the Northern side of the Santa Cruz River.

Figure 6. Photographs of sedimentary facies composing the Santa Cruz-Chico River estuary. (A) Location of the photographs from B to H; (B, C, D) Heterolithic facies showing tidal rhythmites from the inner part of the Chico River (B, C) and from the Santa Cruz River (D). Arrows indicate neap tide periods, according to tidal couplet thickness evolution and/or sedimentary structures. Note the high degree of fragmentation of many clayey layers. Ice crystal growth during freezing seasons is believed to induce this fragmentation; (E), upper intertidal succession with tidal rhythmites (probably neap-spring-neap cycle records) at the Chico River mouth; (F) Salt marsh succession located 1.5 m above (E), with annual tidal rhythmites at the Chico River mouth; (G) Thinly laminated and bioturbated facies of the few tidal mud flat patches preserved along the southern side of the intermediate basin; (H) Thinly laminated facies from mixed tidal flat locally present along the southern side of the intermediate basin.

Figure 7. Results of the sample grain-size analysis (background: Sentinel image Sept. 1, 2022)

Figure 8. Results of the XRD analysis on clay grain size fraction (Background: Sentinel image Sept. 1, 2022) (upstream most samples framed in dark blue, downstream most samples in orange, aeolian samples in pink)

Figure 9. (A) Clay mineral composition of samples; (B) Kübler index vs Esquevin index. Error ±5%. All illites, including the illite-rich samples (green diamonds) fall within the same domains (samples in blue collected in 2018, in pink in 2019).

Figure 10. Results of geochemistry (XRF) analyses on bulk samples. No significant trends or differences are evidenced, neither upstream to downstream (A), nor in relation with sediment facies (B) (note that values for S, Zr, Sr and Ti – right y-axis, are about 1 order less than y-values for Al, Fe and Ca – left y-axis).

Figure 11. Pie diagram presenting the proportion of the foraminifera and testate amoebae species throughout the estuary. The 12 species that account for less than 10% of the assemblage (Miliammina fusca, Spiroplectammina sp., Eggerelloides scaber, Leptohalysis cf. scottii, Textularia cf. agglutinans, Difflugia sp., Bulliminella elegantissima, Cuneata arctica, Parafissurina sp., Spiroplectammina biformis, Trochammina cf. inflata, Cyclopyxis kahli) are grouped as others.

Figure 12. SEM images of observed Testate amoebae (1 to 6) and foraminifera species (7 to 20): Centropyxis platystoma, (1, apertural view and 4, dorsal view); Centropyxis aerophila (2); Cyclopyxis kahli (3); Difflugia oblonga (5); Difflugia lanceolata (6); Cribrostomoides jeffreysii (7); Cuneata arctica (8); Eggerelloides scaber (9); Entzia macrescens (10); Lepidodeuterammina eddystonensis (11); Leptohalysis cf scottii (12); Miliammina fusca (13); Remaneica plicata (14); Spiroplectammina biformis (15); Spiroplectammina sp. (19); Textularia cf. earlandi (17); Textularia cf. agglutinans (18); Trochammina cf. inflata (20). Scale bar is 50µm. SEM shooting: Philippe Recourt, LOG Laboratory.

Figure 13. Seismic profile (Boomer IKB Seistec) shot into the intermediate basin (cf. Fig. 3A for location). (A) raw data; (B) main reflectors underlined; (C) interpreted profile with indication of seismic units.

Figure 14. Examples of GPR profiles (GSSI GPR, 400 MHz antenna) collected in the gravel beach ridges and spits of the North (A) and South (B) of the inlet (cf. Fig. 3B for location).

Fig. 15. Relative proportions of foraminifera and testate amoebae in the SC-CR estuary sediments.

Figure 16. Morphologic and sedimentary domains of the composite Santa Cruz – Chico River estuarine system (background: Sentinel image May 21, 2022, complemented in the North with the Sentinel image Sept.1, 2022 to illustrate the upstream part of the Chico River).

Figure 17. Schematic dip section of the sediment infill of the Santa Cruz estuary system from the Santa Cruz River branch to the tidal inlet and (ebb tidal) delta.

Supplementary material

Table S1. Testate amoebae and foraminifera calculated density for 100 cm^3 of sediment.

Table S2. Comparison of the geochemical results of the present study obtained from the analysis of samples collected into the SC-CR estuary, with geochemical results obtained by Gaiero et al. (2007) on different type of samples (soils, river suspension and bedload, catchment) collected in Patagonia, close to the SC-CR estuary area. RCHI and RSAN are bed sediment samples collected in the Chico and Santa Cruz rivers, upstream of the estuary. TS-CAL and TS-GA are the closest soil samples of the SC-CR estuary area (ca. 200 km to SW and South respectively). ED-CR and ED-PM are eolian dust samples collected 500 km and 1000 km to the North of the SC-CR estuary respectively (see Fig. 1 of Gaiero et al., 2007 for location).

Figure S1. (A) Sentinel image of May 21, 2022 showing a very extended surface plume of suspended sediment expelled from the SC-CR estuary, compared with (B) the most recent reconstructed Digital Elevation Model available for the area (Ezcurra and Schmidt, 2018; Schmidt et al., 2018) picturing a large subaqueous shelf delta (ebb tidal delta).

Table 1. List of samples collected into the Santa Cruz – Chico River estuary with indication of their environment and nature. Cf. Fig. 6 and Fig. 7 for location (Chico R. E: Chico River, SC R. E: Santa Cruz River)

Samples	Location	Environment	Sediment type
SC-2018-01	SC-CR outlet	Mudflat	Mud
SC-2018-02	Chico R.E outlet	Mudflat	Heterolitic facies
SC-2018-03	Chico R.E outlet	Sandflat with 3D dunes	Sand
SC-2018-04	Chico R.E outlet	Sandflat with no dunes	Fine sand
SC-2018-05	Chico R.E. internal	Silty bank	Silt
SC-2018-06	Chico R.E. internal	Mixed flat	Heterolitic facies
SC-2018-07	SC R. E internal	Fluvial bar	Sand
SC-2018-08	SC R. E internal	Fluvial bar	Silty mud
SC-2018-09	Chico R.E. internal	Eolian terrace	Eolian dust
SC-2018-10	Chico R.E. internal	Flood plain	Silt
SC-2018-11	Chico R.E. internal	Mixed flat	Heterolitic facies
SC-2018-12	Chico R.E. internal	Sandflat with 3D dunes	Sand
SC-2018-13	Chico R.E. internal	Flood plain Soil	Black mud
SC-2018-14	Chico R.E. internal	Secondary Tidal channel	Muddy silt
SC-2018-15	SC R. E middle	Mudflat	Mud
SC-2018-16	SC R. E middle	Mixed flat	Heterolitic facies
SC-2018-17	SC R. E middle	Eolian terrace	Eolian dust
SC-2018-18	SC R. E middle	Mudflat	Mud
SC-2019-01	SC-CR outlet	Sandy beach	Sand
SC-2019-02	SC R. E internal	Fluvial bar	Sand

Declaration of interests

☒The authors declare that they have no known competing financial interests or personal relationships that could have appeared to influence the work reported in this paper.

☐The authors declare the following financial interests/personal relationships which may be considered as potential competing interests:

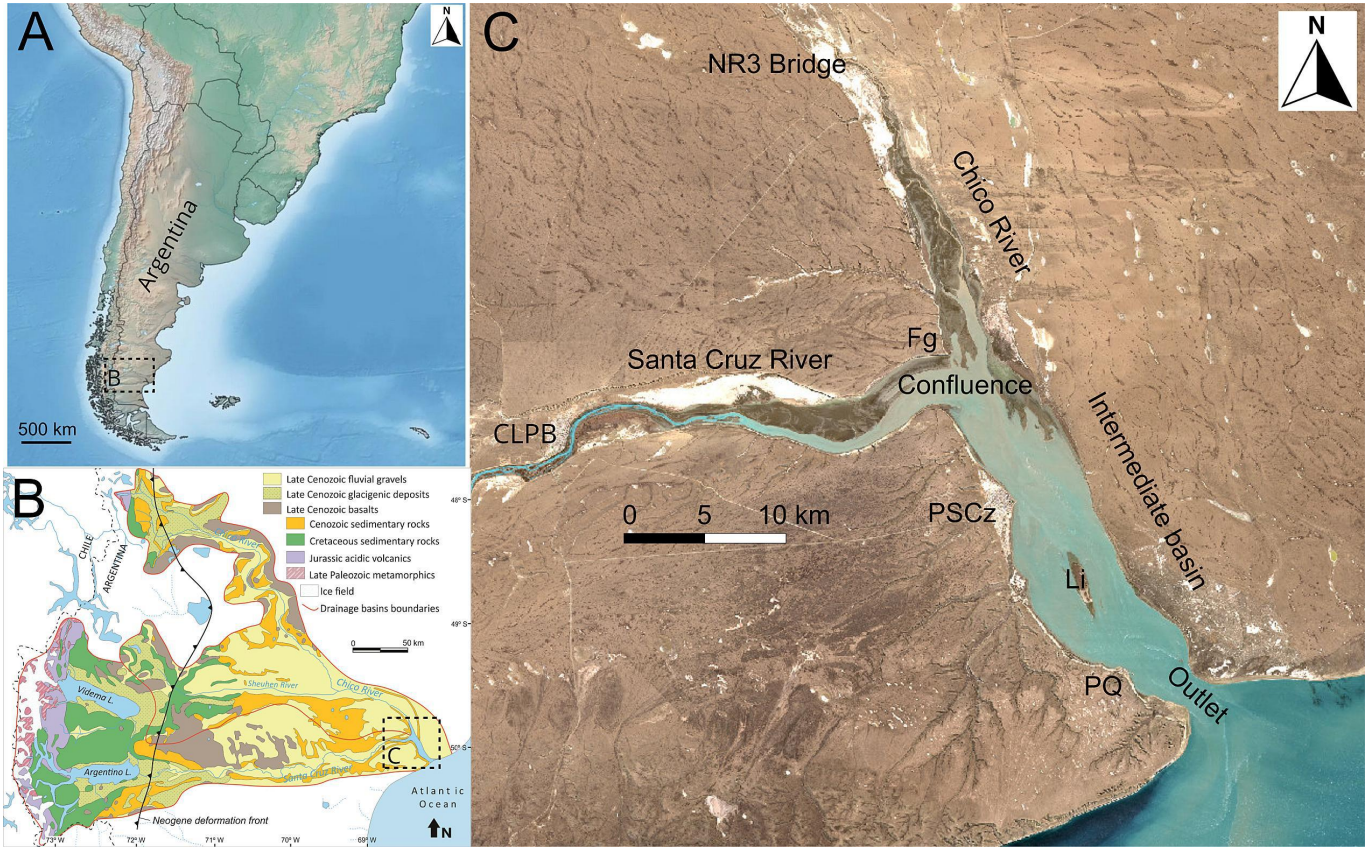
A
N
Argentina
B
500 km
B
Late Cenozoic fluvial gravels
Late Cenozoic glacigenic deposits
Late Cenozoic basalts
Cenozoic sedimentary rocks
Cretaceous sedimentary rocks
Jurassic acidic volcanics
Late Paleozoic metamorphics
Ice field
Drainage basins boundaries
49° S
50 km
CHILE
ARGENTINA
Viedma L.
Chico River
Argentino L.
C
52° S
Atlantic Ocean
N
Neogene deformation front
73° W
72° W
71° W
70° W
69° W
C
N
NR3 Bridge
Chico River
Fg
Santa Cruz River
Confluence
CLPB
0 5 10 km
PSCz
Intermediate basin
Li
PQ
Outlet

Figure 1

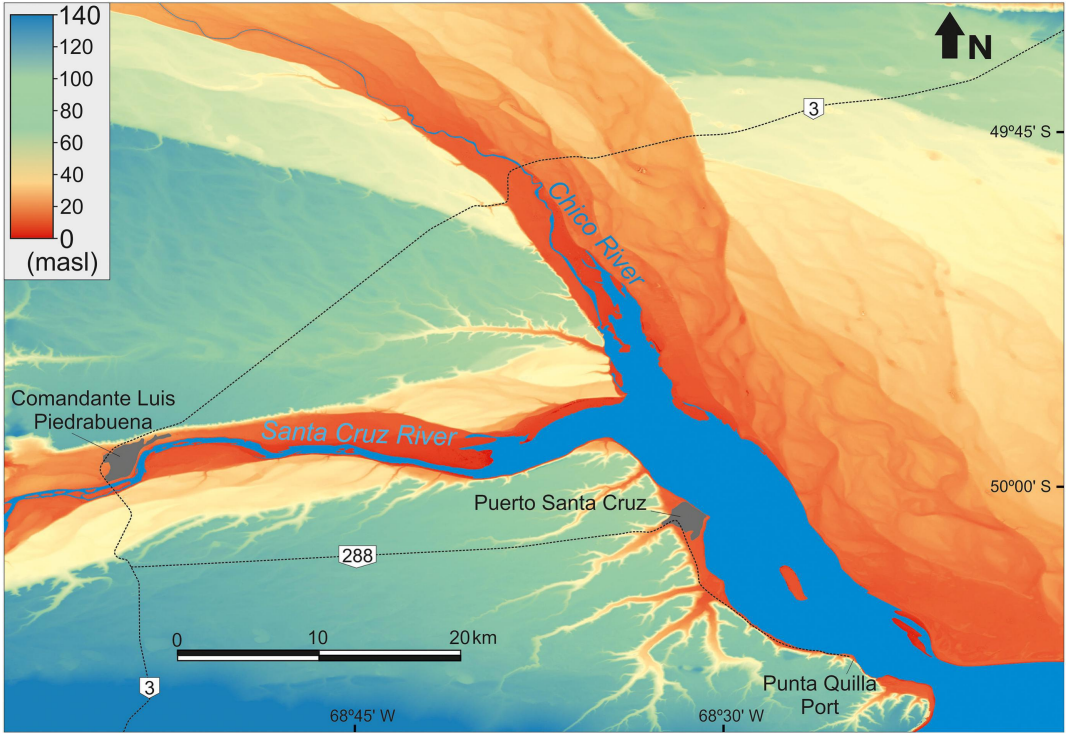
140
120
100
80
60
40
20
0
(masl)
N
3
49°45' S
Chico River
Comandante Luis
Piedrabuena
Santa Cruz River
50°00' S
Puerto Santa Cruz
288
0
10
20km
3
Punta Quilla
Port
68°45' W
68°30' W

Figure 2

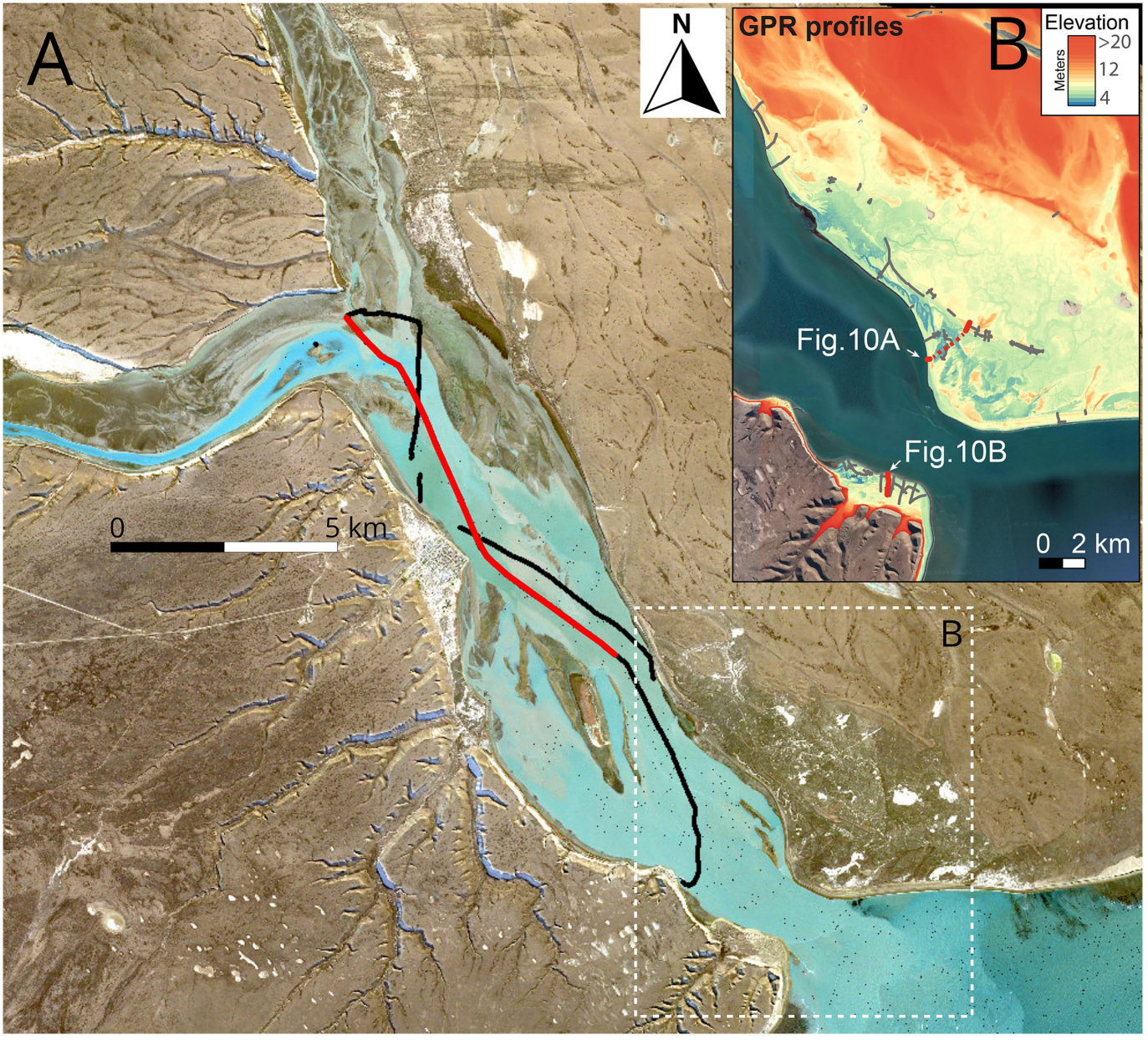
A
N
GPR profiles
B
Elevation
Meters
>20
12
4
Fig.10A
Fig.10B
0 2 km
B
0
5 km

Figure 3

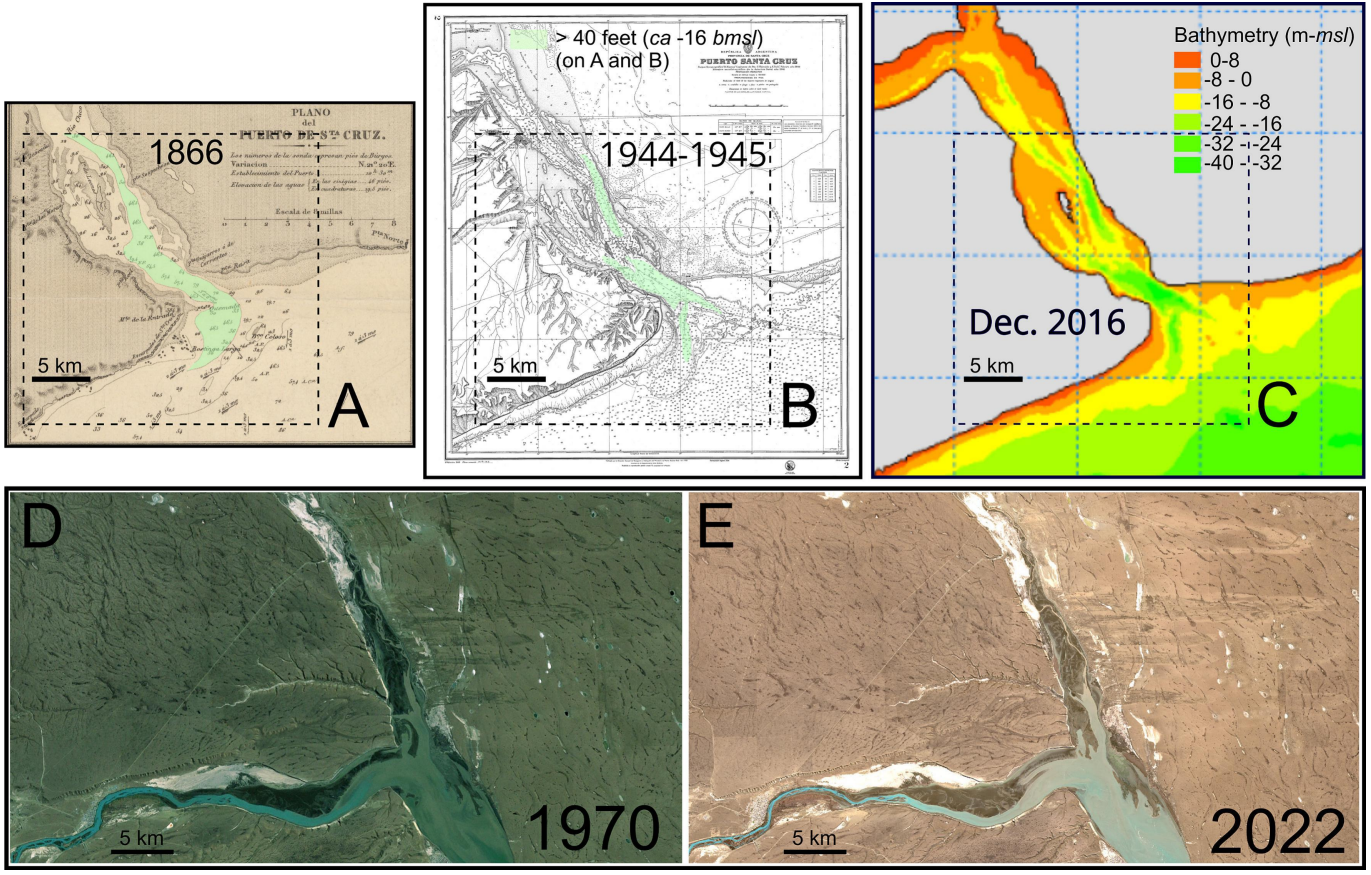
1866
5 km
A
> 40 feet (ca -16 bmsl)
(on A and B)
1944-1945
5 km
B
Bathymetry (m-msl)
0-8
-8 - 0
-16 - -8
-24 - -16
-32 - -24
-40 - -32
Dec. 2016
5 km
C
D
5 km
1970
E
5 km
2022

Figure 4

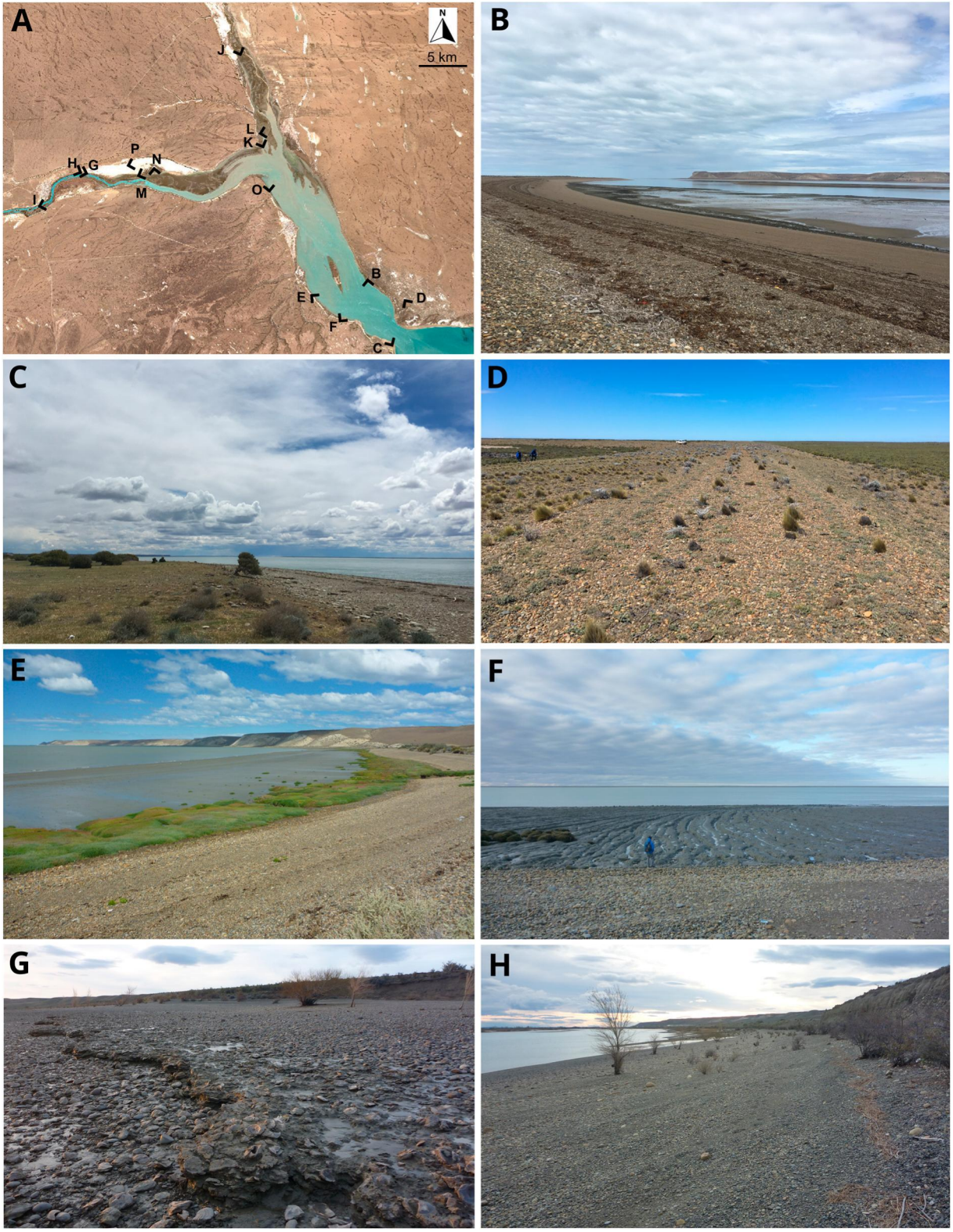

Figure 5AH

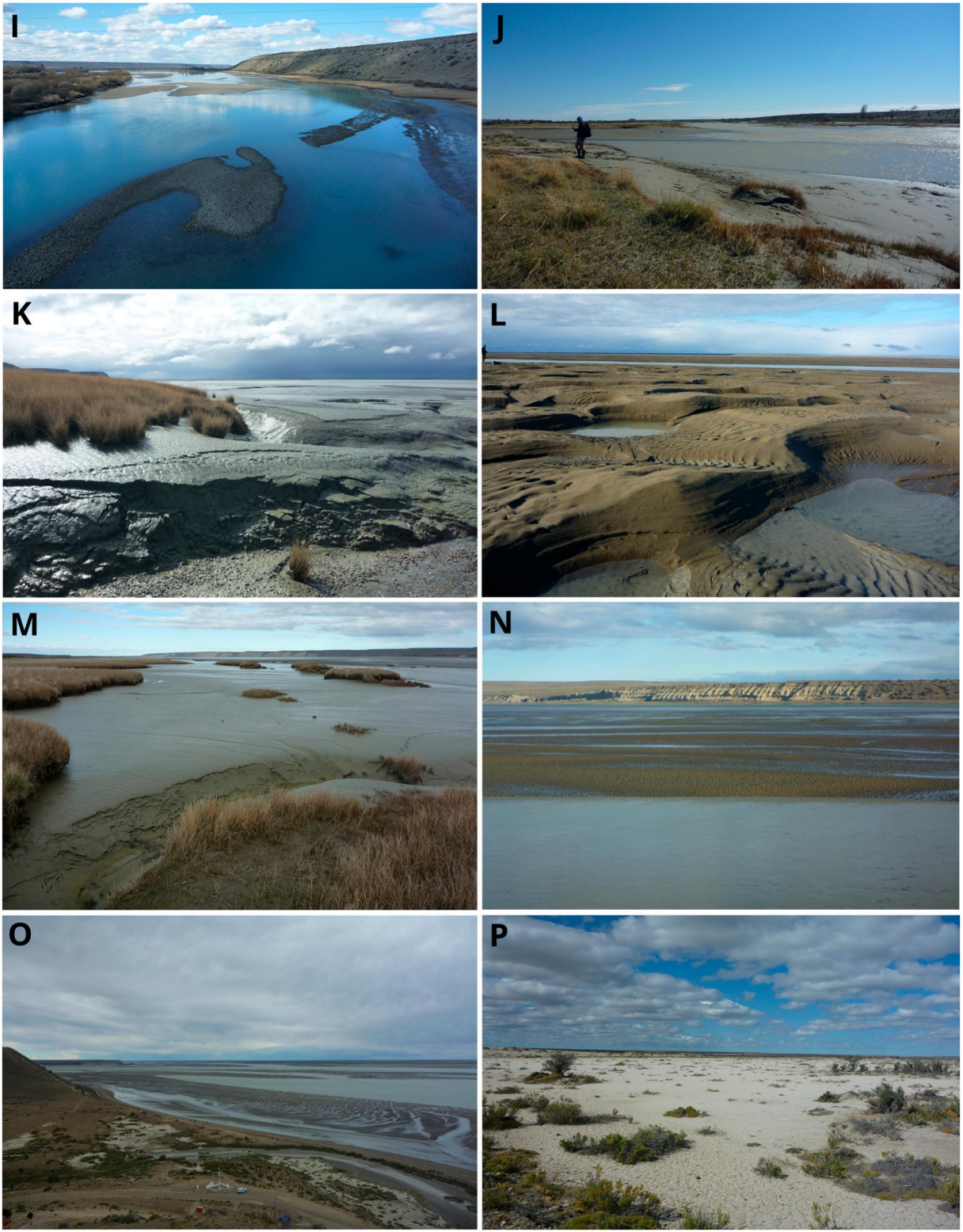

Figure 5IP

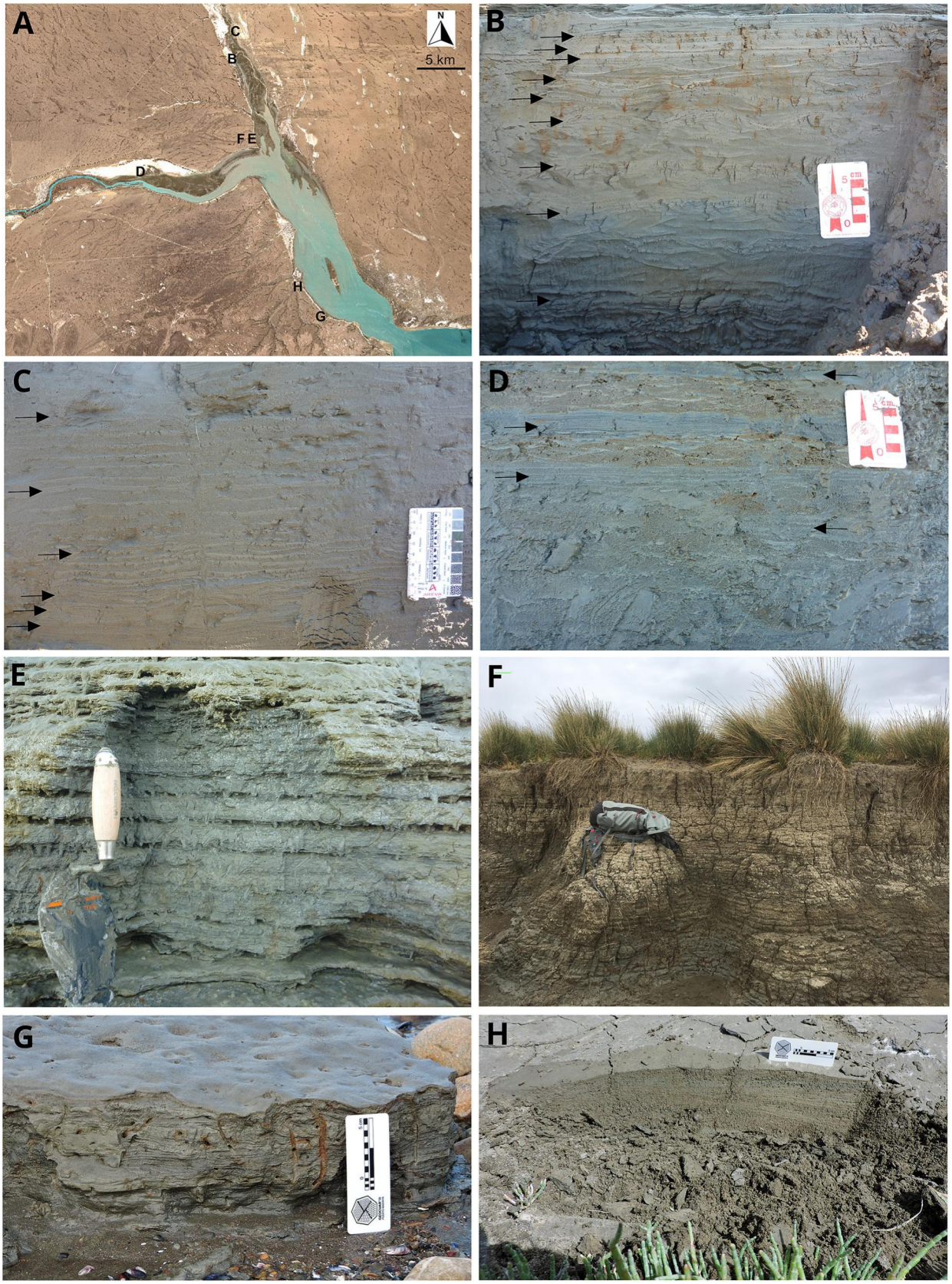

Figure 6


5
6
9
10
14
11
13
12
N
5 km
17
18
4
3
2
15
16
8
7
1
all samples
very fine to fine sands
med. to coarse silts
med. sands
0.1
1
10
100
1000
diameter (μm)

Figure 7

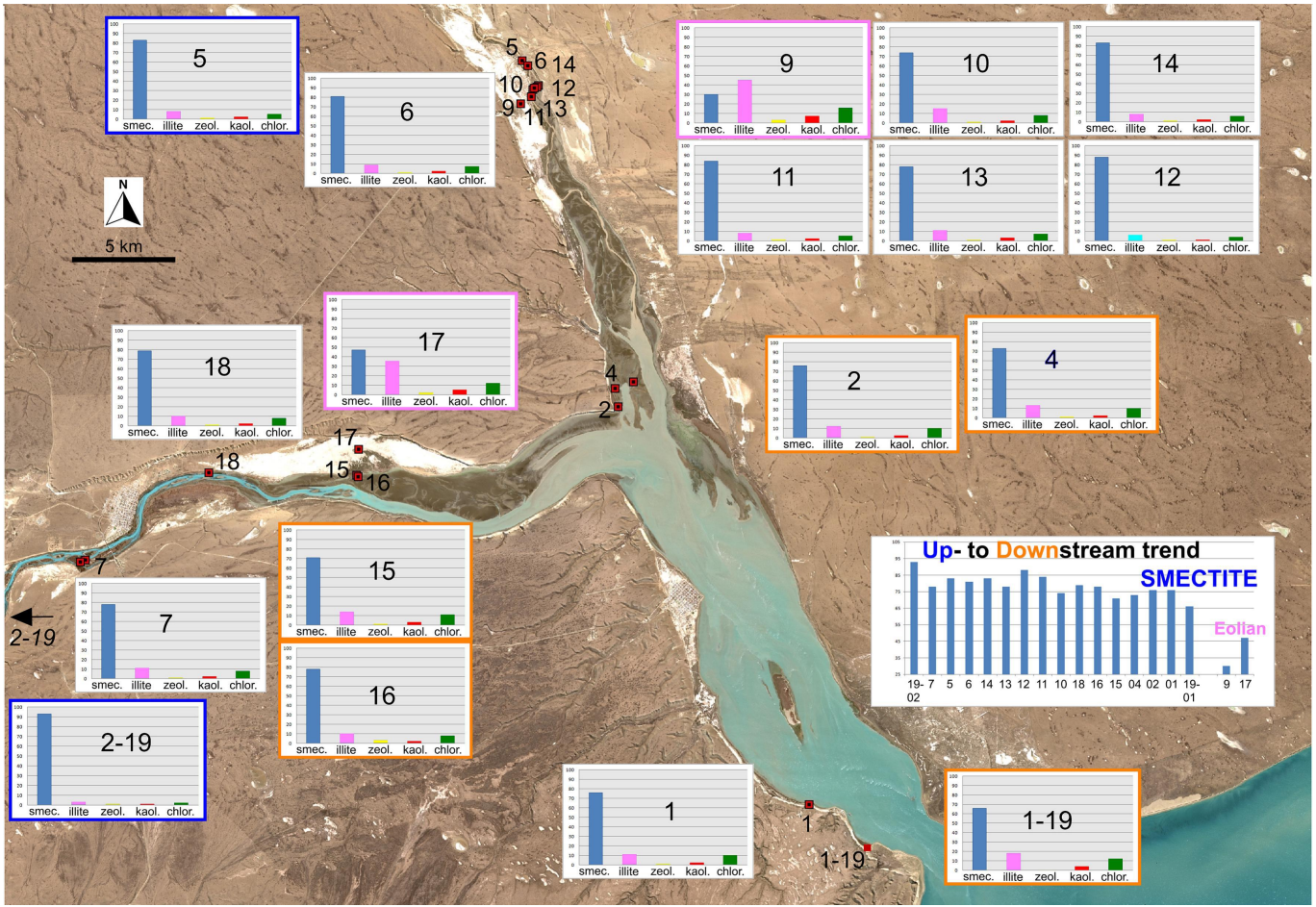
5
6
9
10
14
11
13
12
18
17
2
4
15
16
7
2-19
1
1-19
smec. illite zeol. kaol. chlor.
N
5 km
Up- to Downstream trend
SMECTITE
Eolian
19-02 7 5 6 14 13 12 11 10 18 16 15 04 02 01 19-01 9 17

Figure 8

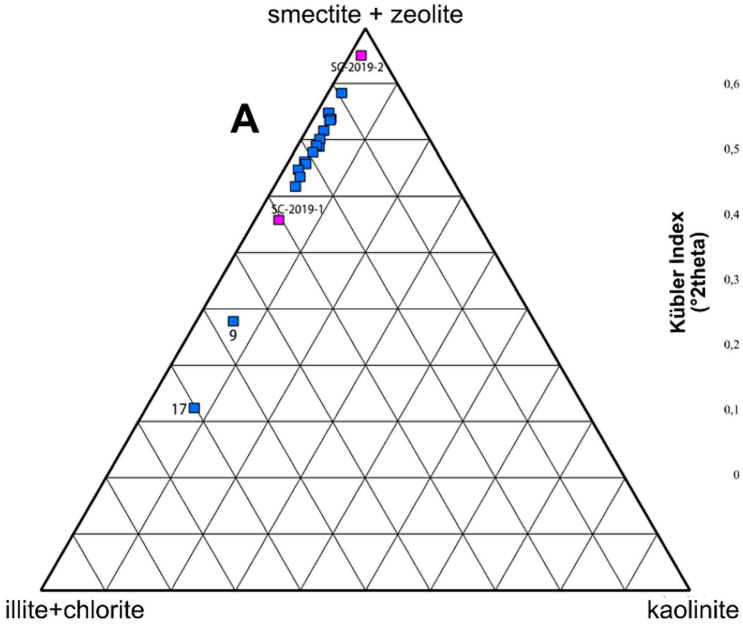
smectite + zeolite
A
SC-2019-2
SC-2019-1
9
17
illite+chlorite
kaolinite

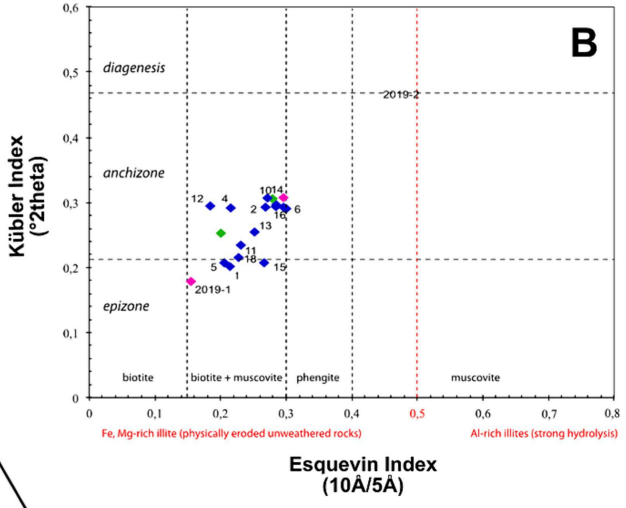
B
diagenesis
anchizone
epizone
2019-2
2019-1
12
4
10
14
2
16
6
13
11
18
5
1
15
biotite
biotite + muscovite
phengite
muscovite
Kübler Index
(°2theta)
0,6
0,5
0,4
0,3
0,2
0,1
0
0
0,1
0,2
0,3
0,4
0,5
0,6
0,7
0,8
Fe, Mg-rich illite (physically eroded unweathered rocks)
Al-rich illites (strong hydrolysis)
Esquevin Index
(10Å/5Å)

Figure 9

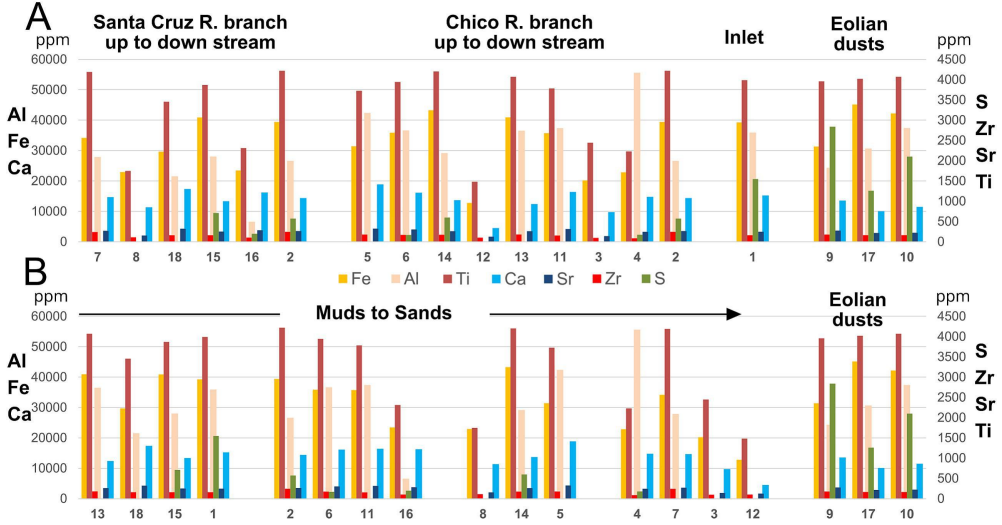
A
Santa Cruz R. branch up to down stream
Chico R. branch up to down stream
Inlet
Eolian dusts
ppm
Al
Fe
Ca
S
Zr
Sr
Ti
7 8 18 15 16 2 5 6 14 12 13 11 3 4 2 1 9 17 10
Fe Al Ti Ca Sr Zr S
B
Muds to Sands
Eolian dusts
13 18 15 1 2 6 11 16 8 14 5 4 7 3 12 9 17 10

Figure 10

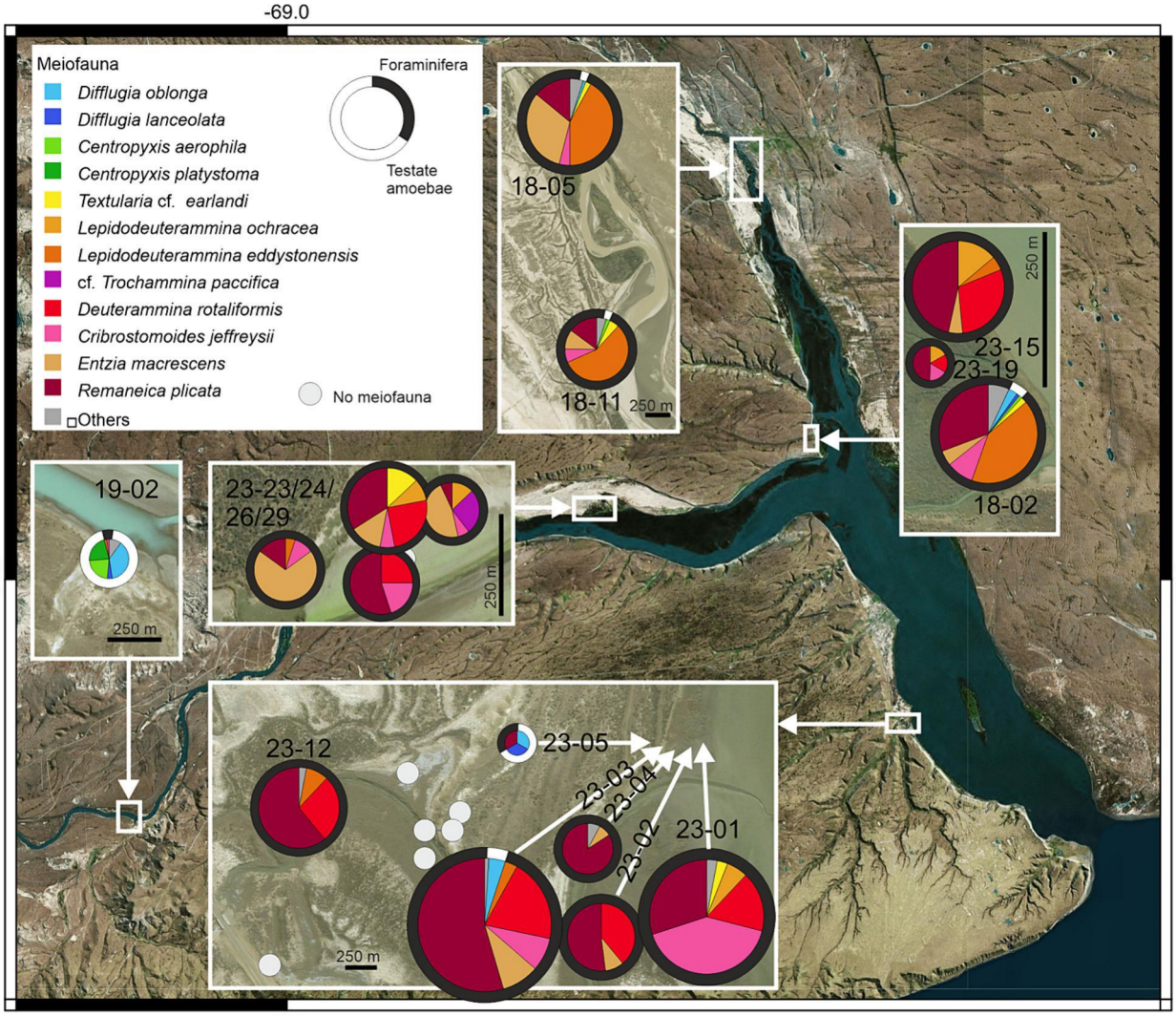
-69.0
-50.0
Meiofauna
Difflugia oblonga
Difflugia lanceolata
Centropyxis aerophila
Centropyxis platystoma
Textularia cf. earlandi
Lepidodeuterammina ochracea
Lepidodeuterammina eddystonensis
cf. Trochammina paccifica
Deuterammina rotaliformis
Cribrostomoides jeffreysii
Entzia macrescens
Remaneica plicata
Others
Foraminifera
Testate amoebae
No meiofauna
18-05
18-11
250 m
23-15
23-19
18-02
19-02
23-23/24/ 26/29
23-12
23-05
23-03
23-04
23-02
23-01

Figure 11

Figure 12

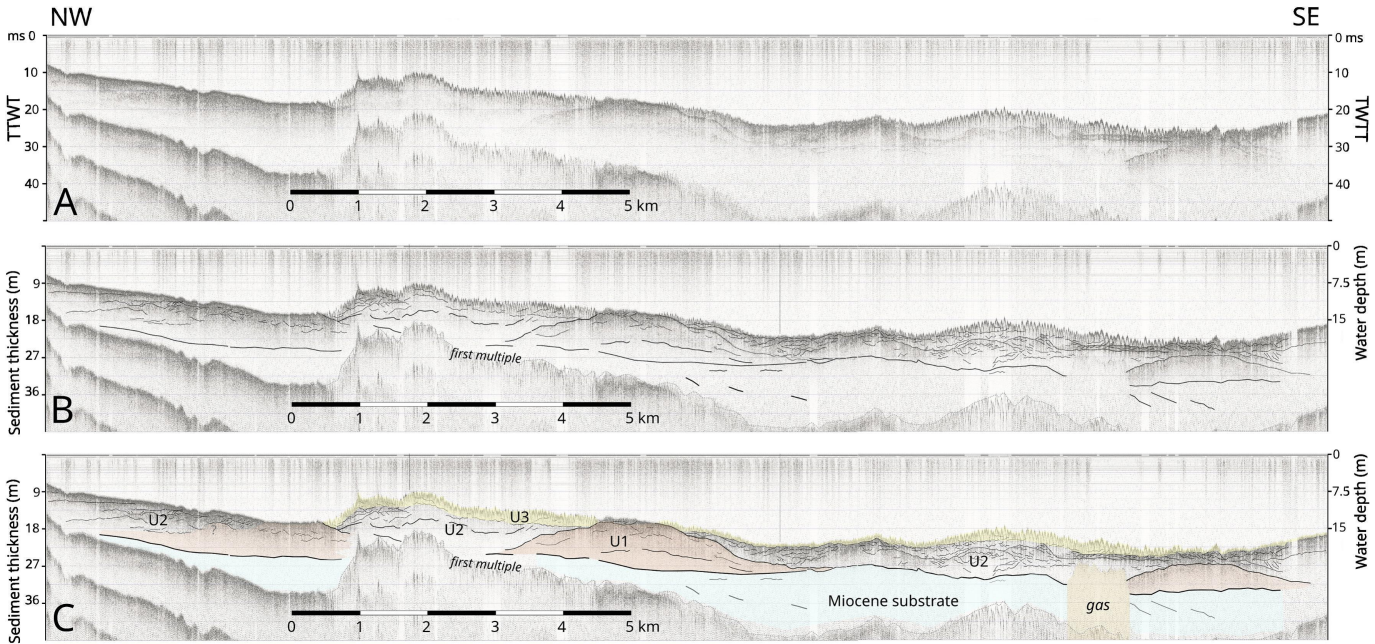
NW
SE
ms 0
TTWT
10
20
30
40
0 ms
TWTT
A
0 1 2 3 4 5 km
Sediment thickness (m)
9
18
27
36
0
7.5
15
Water depth (m)
first multiple
B
C
U2
U3
U1
Miocene substrate
gas

Figure 13

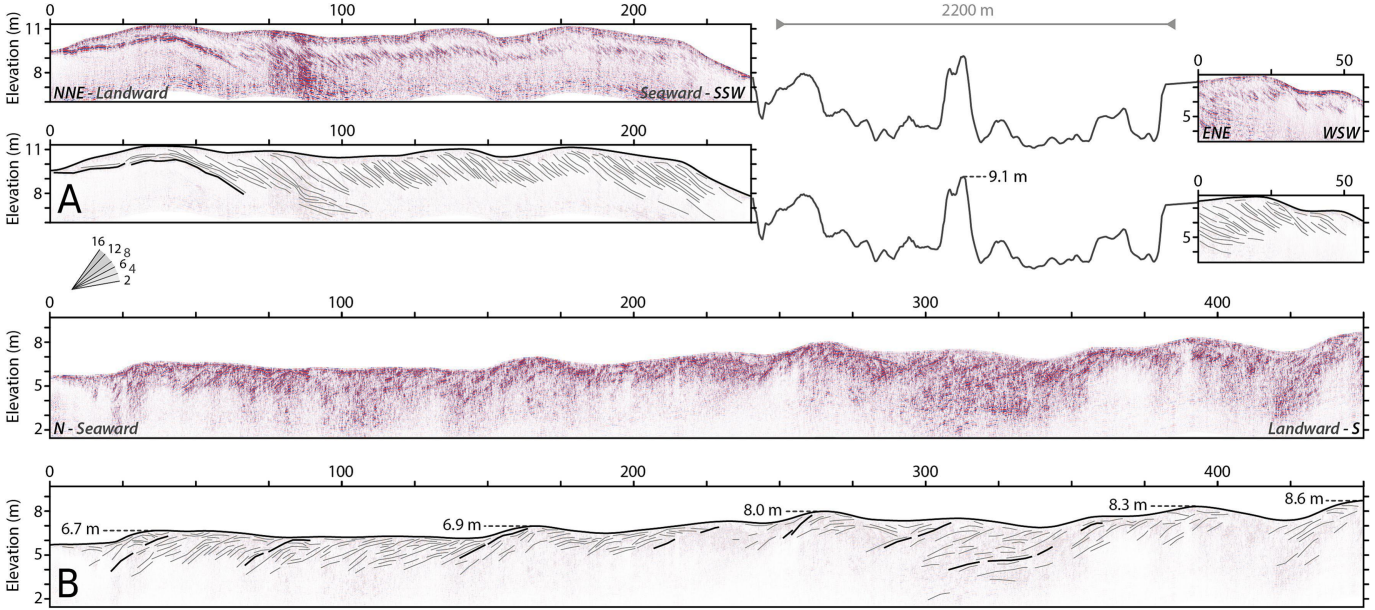
0
100
200
2200 m
Elevation (m)
11
8
NNE - Landward
Seaward - SSW
0
50
5
ENE
WSW
A
9.1 m
16
12
8
6
4
2
300
400
5
2
N - Seaward
Landward - S
6.7 m
6.9 m
8.0 m
8.3 m
8.6 m
B

Figure 14

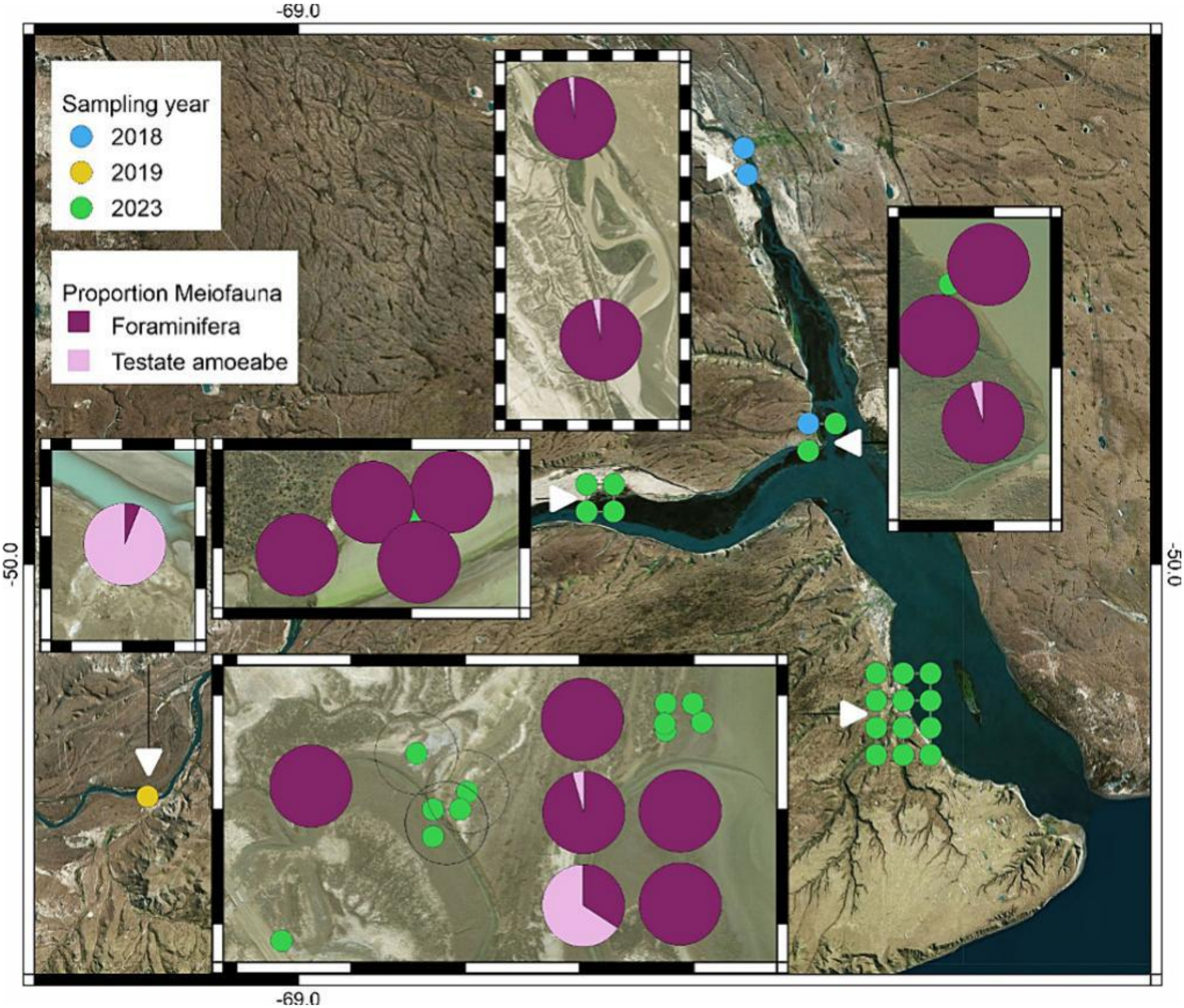
-69.0
Sampling year
2018
2019
2023
Proportion Meiofauna
Foraminifera
Testate amoeabe
-50.0
-50.0
-69.0

Figure 15

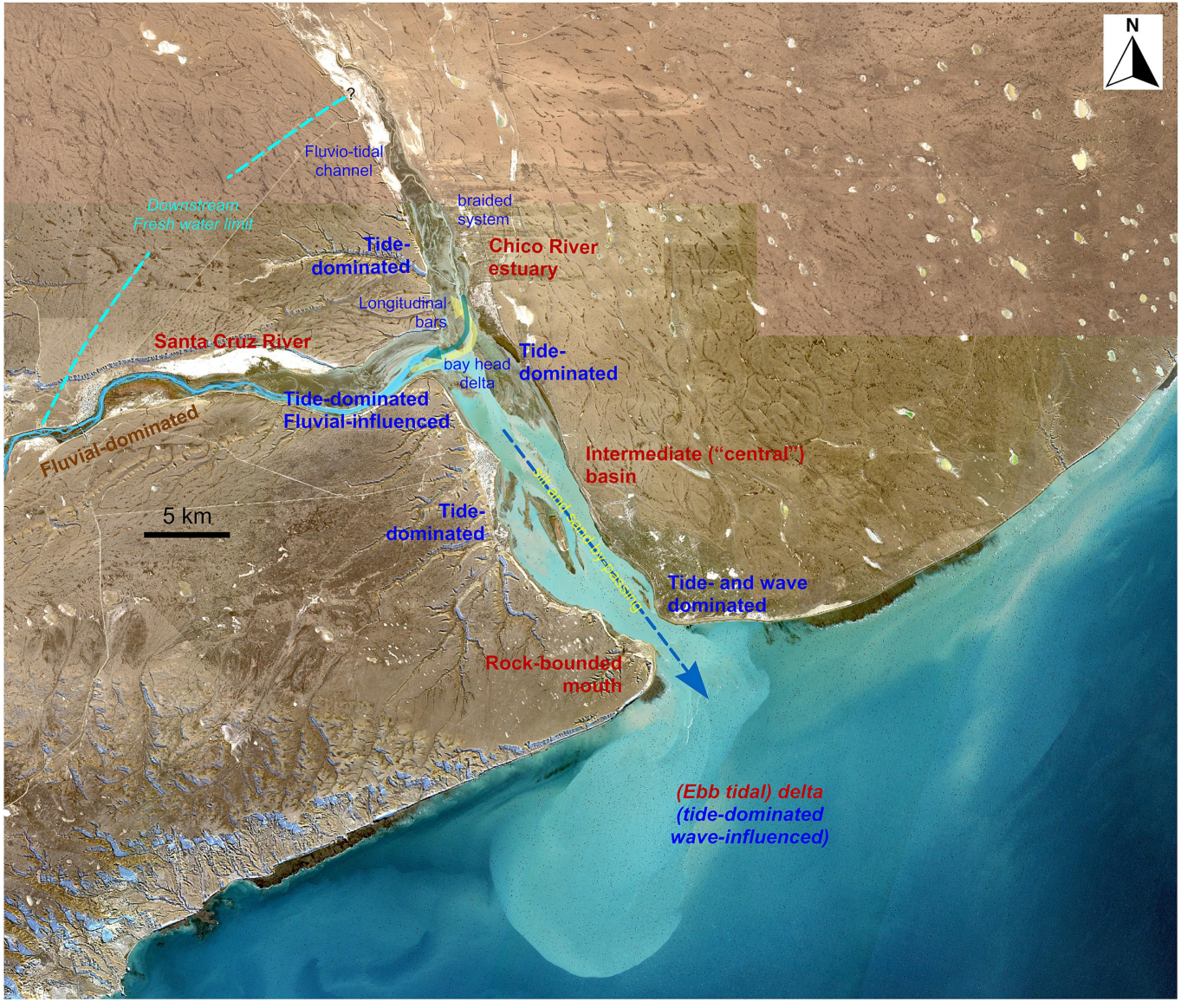
N
?
Fluvio-tidal channel
Downstream Fresh water limit
braided system
Tide-dominated
Chico River estuary
Longitudinal bars
Santa Cruz River
bay head delta
Tide-dominated
Tide-dominated Fluvial-influenced
Fluvial-dominated
Intermediate ("central") basin
5 km
Tide-dominated
Tide- and wave dominated
Rock-bounded mouth
(Ebb tidal) delta (tide-dominated wave-influenced)

Figure 16

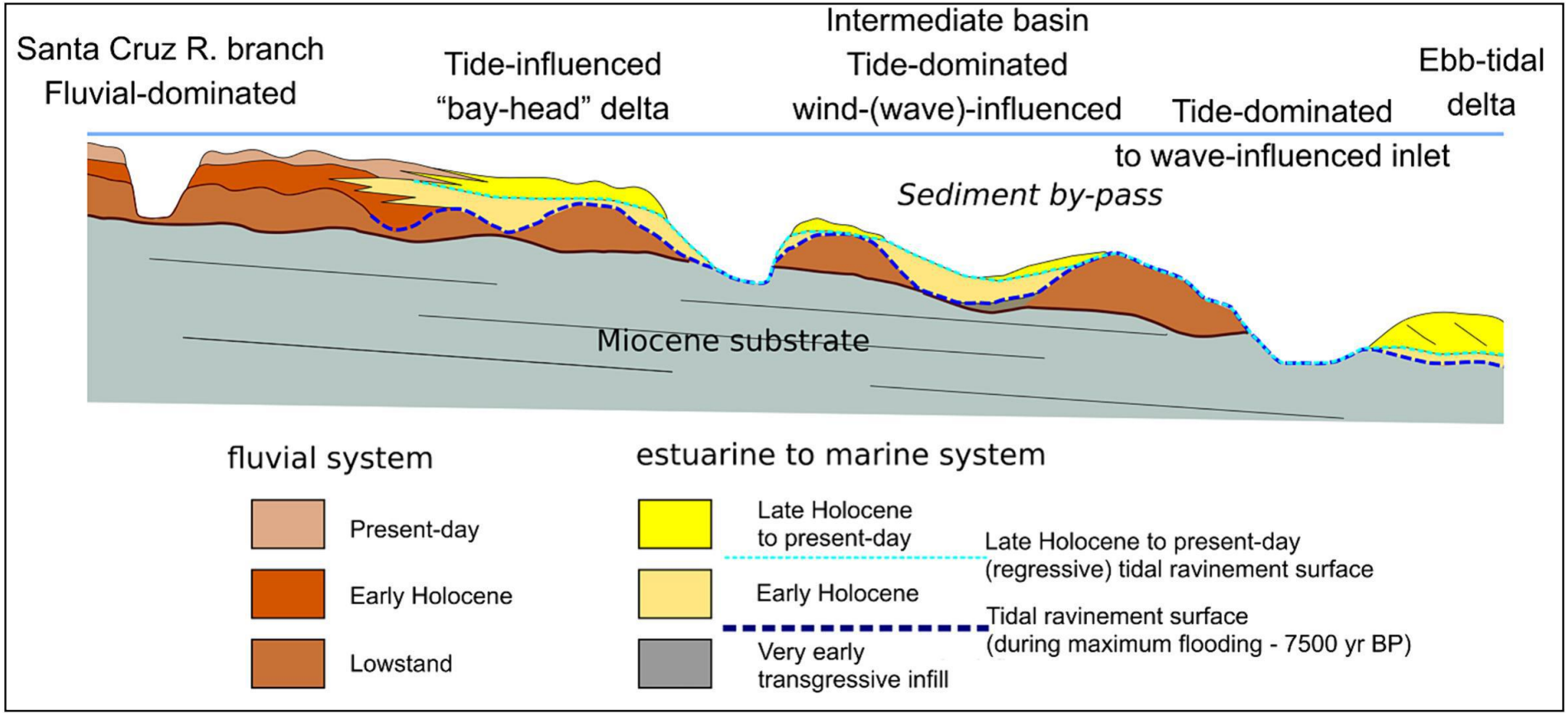
Santa Cruz R. branch
Fluvial-dominated
Tide-influenced
“bay-head” delta
Intermediate basin
Tide-dominated
wind-(wave)-influenced
Tide-dominated
to wave-influenced inlet
Ebb-tidal
delta
Sediment by-pass
Miocene substrate
fluvial system
Present-day
Early Holocene
Lowstand
estuarine to marine system
Late Holocene
to present-day
Early Holocene
Very early
transgressive infill
Late Holocene to present-day
(regressive) tidal ravinement surface
Tidal ravinement surface
(during maximum flooding - 7500 yr BP)

Figure 17